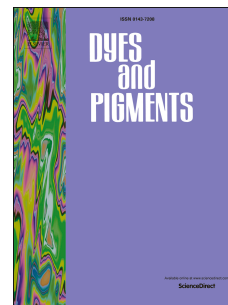


Accepted Manuscript

New Acceptor- π -Porphyrin- π -Acceptor Systems for Solution-Processed Small Molecule Organic Solar Cells

Susana Arrechea, Agustín Molina-Ontoria, Ana Aljarilla, Pilar de la Cruz, Fernando Langa, Luis Echegoyen



PII: S0143-7208(15)00167-9

DOI: [10.1016/j.dyepig.2015.04.037](https://doi.org/10.1016/j.dyepig.2015.04.037)

Reference: DYPI 4759

To appear in: *Dyes and Pigments*

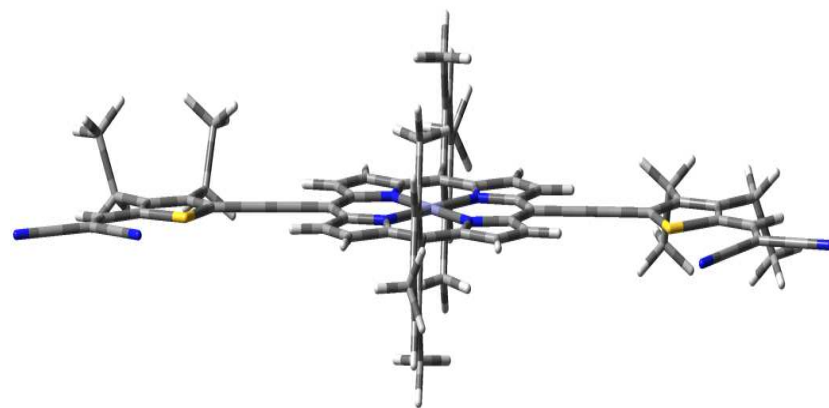
Received Date: 23 March 2015

Revised Date: 23 April 2015

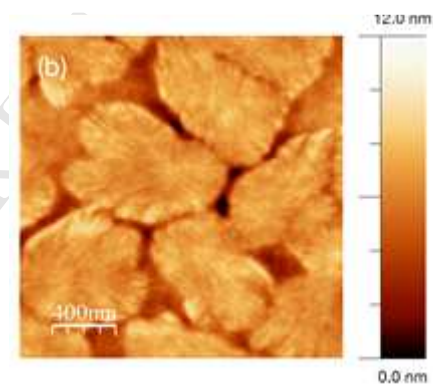
Accepted Date: 27 April 2015

Please cite this article as: Arrechea S, Molina-Ontoria A, Aljarilla A, de la Cruz P, Langa F, Echegoyen L, New Acceptor- π -Porphyrin- π -Acceptor Systems for Solution-Processed Small Molecule Organic Solar Cells, *Dyes and Pigments* (2015), doi: 10.1016/j.dyepig.2015.04.037.

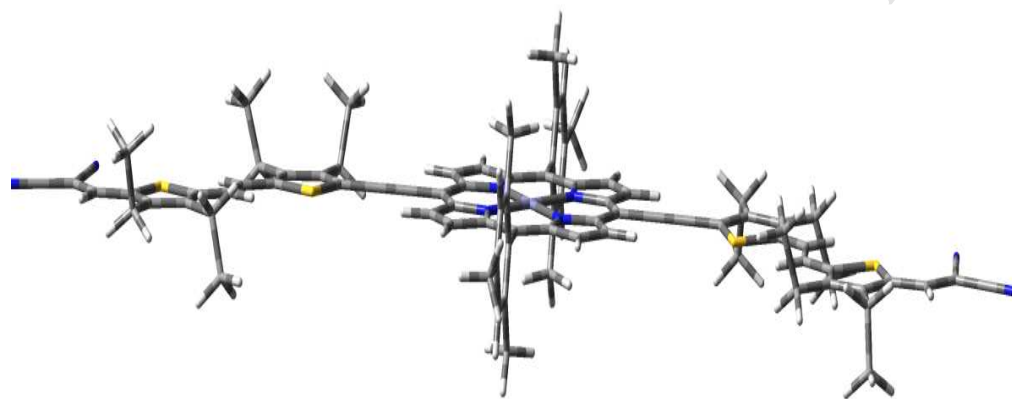
This is a PDF file of an unedited manuscript that has been accepted for publication. As a service to our customers we are providing this early version of the manuscript. The manuscript will undergo copyediting, typesetting, and review of the resulting proof before it is published in its final form. Please note that during the production process errors may be discovered which could affect the content, and all legal disclaimers that apply to the journal pertain.



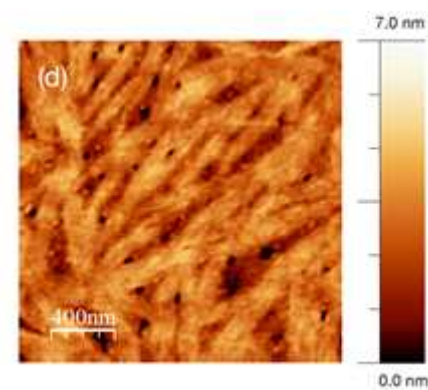
1a $\eta = 1.36\%$



PC₆₁BM



1b $\eta = 3.16\%$



PC₇₁BM

New Acceptor- π -Porphyrin- π -Acceptor Systems for Solution-Processed Small Molecule Organic Solar Cells

Susana Arrechea,^a Agustín Molina-Ontoria,^b Ana Aljarilla,^a Pilar de la Cruz,^a Fernando Langa^{a,*} and Luis Echegoyen^{b,*}

^a *Universidad de Castilla-La Mancha. Institute of Nanoscience, Nanotechnology and Molecular Materials (INAMOL), Campus de la Fábrica de Armas, Toledo, Spain.*

^b *Department of Chemistry, University of Texas at El Paso, El Paso, TX 79968, USA.*

Abstract: Two new conjugated acceptor-donor-acceptor (A- π -D- π -A) compounds having a Zn-porphyrin acting as donor and linked by ethynylenes to one or two units of thienylenevinylene and capped by dicyanovinylene groups as acceptor units have been synthesized and their photophysical and electrochemical properties were investigated. These compounds were used as donor materials and PC₆₁BM and PC₇₁BM were used as acceptors in solution-processed bulk-heterojunction (BHJ) organic solar cells and the best photoconversion efficiency (PCE) obtained was 3.21%.

Keywords: Photovoltaics, bulk heterojunction solar cells, small molecule, porphyrin.

Introduction

Efficient production of clean and sustainable energy is one of the most important scientific challenges that the world faces today. Sunlight is the most abundant and one of the cleanest sources of energy, thus the efficient utilization of solar energy to prepare solar cells has attracted much attention from the scientific community.¹⁻³ The development of efficient organic photovoltaic (OPV) solar cells has attracted considerable interest as potential alternative solar energy sources to silicon-based solar cells, because of their distinct advantages of solution processability, low-cost, flexibility and roll-to-toll production possibilities. The bulk heterojunction (BHJ) approach is the most efficient to date, which consists of a nanometer scale interpenetrating network of an electron-accepting, typically fullerene, phase and a light-harvesting electron-donor phase, such as a polymer or a small molecule. Polymer solar cells (PSCs) underwent significant progress in the past decades, thanks to the judicious design of narrow band-gap copolymers, optimization of the nanoscale morphologies of the photoactive layers and enhanced carriers mobilities, which have led to power conversion efficiencies (PCEs) of 10% for single-junction PSCs^{4,5} and up to 11% for tandem PSCs.⁶ Nonetheless, there are issues with the synthesis of conjugated polymers for photovoltaic applications, such as difficult purification, poor batch-to-batch reproducibility and so on.

Solution processed small-molecule organic solar cells (SMBHJ), are an emerging alternative to the polymer counterparts, and these have rapidly developed in recent years, which offer potential advantages, such as better defined structures, easier purification and better reproducibility.⁶⁻⁹ Thus far, power conversion efficiencies exceeding 9% have been reported for solution-processed small molecule single junction devices.¹⁰⁻¹⁵

Inspired by natural photosynthetic organisms, where chlorophylls absorb light for energy conversion, and because of intense Soret band at around 400 nm and the Q bands close to 600 nm, porphyrins and their derivatives are excellent building blocks for the construction of light harvesting architectures.¹⁶ Porphyrins are among the best sensitizers in Dye Sensitized Solar cells (DSSCs)¹⁷⁻²² showing performances as high as 12%.²³ However, the utilization of porphyrins as active materials in solution-processed BHJ solar cells have been limited²⁴⁻³³ despite their natural tendency to form aggregates by π - π stacking interactions.³⁴

In this article we report the synthesis of two new conjugated acceptor-donor-acceptor (A- π -D- π -A) molecules **1a** and **1b** (Figure 1), along with their photophysical and electrochemical properties, as well as their performance in solution-processed SMBHJ. Both compounds were used as the p type layer with the Zn-porphyrin core acting as a donor linked by ethynyls to one or two units of thienylenevinylene and capped by dicyanovinylene groups as acceptor units. Ethynyls were chosen to make the systems planar and hexyl chains were attached on the thiophene units to enhance their solubility. PC₆₁BM and PC₇₁BM were used as acceptor components in the devices.

Figure 1.

Experimental Section

2.1. Experimental details are given in the Supporting Information.

2.2. Synthetic Procedures.

General synthetic procedure for 3a,b.³⁵ To a solution of **5a,b**³⁶ (1 eq) in carbon tetrachloride (CCl₄, 1.25 mL/mmol) was added PhI(OCOFCF₃)₂ (0.55 eq) and molecular iodine (I₂, 0.5 eq). The mixture was stirred at room temperature. The reaction was quenched with a saturated solution of sodium thiosulfate (Na₂SO₃ sat.) while stirring for 15 min and extracted with CH₂Cl₂. The combined organic phases were dried over anhydrous MgSO₄ and filtered. The solvent was removed by rotary evaporation.

5-Iodo-3,4-dihexyl-2-thiophencarboxaldehyde (3a). Using the general procedure previously described, **5a** (1.8 mmol, 500 mg) was reacted with $\text{PhI}(\text{OCOCF}_3)_2$ (1.0 mmol, 416 mg) and I_2 (0.9 mmol, 226 mg) in 2.2 mL of CCl_4 . The product was purified by column chromatography (silica gel, hexane- CHCl_3 , 7:3). **3a** was obtained as a yellow oil (610 mg, 1.51 mmol, 84% yield). ^1H NMR (400 MHz, CDCl_3) δ /ppm: 9.90 (s, 1H), 2.94-2.90 (m, 2H), 2.57-2.53 (m, 2H), 1.64-1.57 (m, 4H), 1.39-1.31 (m, 12H), 0.93-0.88 (m, 6H). ^{13}C NMR (100 MHz, CDCl_3) δ /ppm: 181.2, 150.5, 148.4, 143.0, 89.7, 32.3, 31.5, 31.4, 30.6, 29.7, 29.3, 29.3, 27.8, 22.6, 22.5, 14.1, 14.0. MALDI-TOF MS (m/z): $[\text{M}]^+$ calculated for $\text{C}_{17}\text{H}_{27}\text{IOS}$: 406.08; found: 406.08. FT-IR (ATR) ν/cm^{-1} : 2923, 2854, 1654, 1523, 1461, 1427, 1365, 1222, 1126, 1079, 721, 674.

(E)-1-(5-Formyl-3,4-dihexyl-2-thienyl)-2-(5-iodo-3',4'-dihexyl-2'-thienyl)ethylene (3b). Using the general procedure previously described, **5b** (0.6 mmol, 338 mg) was reacted with $\text{PhI}(\text{OCOCF}_3)_2$ (0.3 mmol, 142 mg), I_2 (0.3 mmol, 77 mg) in 0.75 mL of CCl_4 . The product was purified by column chromatography (silica gel, hexane- CHCl_3 , 3:2). **3b** was obtained as a yellow oil (255 mg, 0.37 mmol, 62% yield). ^1H NMR (400 MHz, CDCl_3) δ /ppm: 9.98 (s, 1H), 7.19 (d, 1H, $J = 15.5$ Hz), 6.97 (d, 1H, $J = 15.5$ Hz), 2.84 (t, 2H, $J = 7.7$ Hz), 2.64 (t, 2H, $J = 7.7$ Hz), 2.58 (t, 2H, $J = 7.7$ Hz), 2.49 (t, 2H, $J = 7.7$ Hz), 1.50-1.27 (m, 32H), 0.94-0.88 (m, 12H). ^{13}C NMR (100 MHz, CDCl_3) δ /ppm: 181.9, 153.0, 147.7, 146.6, 141.8, 141.6, 141.0, 134.8, 123.1, 118.8, 75.5, 32.3, 31.6, 31.5, 31.4, 31.1, 31.0, 29.8, 29.3, 27.9, 27.1, 26.4, 22.6, 22.5, 14.1, 14.05. MALDI-TOF MS (m/z): $[\text{M}]^+$ calculated for $\text{C}_{35}\text{H}_{55}\text{IOS}_2$: 682.27; found: 683.49. FT-IR (ATR) ν/cm^{-1} : 2923, 2850, 1654, 1600, 1523, 1461, 1403, 1375, 1249, 1211, 933, 725, 678, 663.

Synthesis of 5,15-dimesitylporphyrin.³⁷ A solution of corresponding dipyrromethane³⁸ (14.4 mmol, 2.10 g) and 2,4,6-trimethylbenzaldehyde (14.4 mmol, 2.1 mL) in 1.40 L of CHCl_3 was treated with $\text{BF}_3\text{O}(\text{C}_2\text{H}_5)_2$ (4.7 mmol, 0.6 mL). The mixture was stirred for 3 h. DDQ (21.5 mmol, 4.9 g) was added and the reaction mixture was stirred for 1 h. Et_3N (2.0 mL) was added and stirred during 30 min. The solvent was removed by rotary evaporation and the solid was purified by column chromatography (silica gel, hexane- CHCl_3 , 1:1). 5,15-Dimesitylporphyrin was obtained as a purple solid (1400 mg, 2.56 mmol, 35% yield). ^1H NMR (400 MHz, CDCl_3) δ /ppm: 10.25 (s, 2H), 9.35 (d, 4H, $J = 4.5$ Hz), 8.91 (d, 4H, $J = 4.5$ Hz), 7.35 (s, 4H), 2.69 (s, 6H), 1.87 (s, 12H), -3.04 (s, 2H). ^{13}C NMR (100 MHz, CDCl_3) δ /ppm: 146.8, 145.4, 139.5, 137.8, 137.6, 131.8, 130.0, 127.8, 117.3, 104.6, 21.7, 21.5. MALDI-TOF MS (m/z): $[\text{M}]^+$ calculated for $\text{C}_{38}\text{H}_{34}\text{N}_4$: 546.09; found: 546.28. FT-IR (ATR) ν/cm^{-1} : 3305, 1828, 1604, 1411, 1373, 1319, 1234, 1052, 950, 852, 782, 736, 694, 617.

Synthesis of [5,15-dimesitylporphyrinato] zinc (II).³⁹ To a solution of 5,15-dimesitylporphyrin (2.5 mmol, 1.35 g) in 209 mL of CHCl_3 , was added a solution of

Zn(OAc)₂·2H₂O (12.3 mmol, 2.26 g) in 6.2 mL of MeOH. The mixture was stirred 18 hours. The reaction was quenched with water and extracted with CHCl₃ (3 x 100 mL). The combined organic extract was dried over anhydrous MgSO₄ and filtered. The solvent was removed by rotary evaporation. The product was purified by column chromatography (silica gel, hexane-CHCl₃, 1:1). The product [5,15-dimesitylporphyrinato] zinc (II), was obtained as a purple solid (1510 mg, 2.47 mmol, 99% yield). ¹H NMR (400 MHz, CDCl₃) δ/ppm: 10.27 (s, 2H), 9.41 (d, 4H, *J* = 4.4 Hz), 9.00 (d, 4H, *J* = 4.4 Hz), 7.35 (s, 4H), 2.69 (s, 6H), 1.85 (s, 12H). ¹³C NMR (100 MHz, CDCl₃) δ/ppm: 149.8, 149.4, 139.3, 138.8, 135.7, 132.1, 131.3, 127.7, 118.2, 105.5, 21.7, 21.5. MALDI-TOF MS (*m/z*): [M]⁺ calculate for C₃₈H₃₂N₄Zn: 608.57; found: 608.19. FT-IR (ATR) ν/cm⁻¹: 1816, 1608, 1438, 1388, 1318, 1211, 1052, 856, 786, 728, 701, 617.

Synthesis of [5,15-dibromo-10,20-dimesitylporphyrinato] zinc (II). To a solution of [5,15-dimesitylporphyrinato] zinc (II) (1.5 mmol, 920 mg) in 80 mL of CHCl₃, *N*-bromosuccinimide (NBS) (3.0 mmol, 536 mg) and 1 mL of pyridine were added. The mixture was stirred 30 minutes and quenched with acetone. The solvent was removed by rotary evaporation and the solid was purified by column chromatography (silica gel, hexane-CHCl₃, 7:3). The product [5,15-dibromo-10,20-dimesitylporphyrinato] zinc (II) was obtained as a purple solid (1117 mg, 1.45 mmol, 98% yield). ¹H NMR (400 MHz, CDCl₃) δ/ppm: 9.59 (d, 4H, *J* = 4.6 Hz), 8.71 (d, 4H, *J* = 4.6 Hz), 7.80 (s, 4H), 2.65 (s, 6H), 1.80 (s, 12H). ¹³C NMR (100 MHz, CDCl₃) δ/ppm: 150.5, 149.9, 139.1, 138.8, 137.6, 133.3, 132.0, 127.7, 122.3, 120.1, 104.1, 55.4, 21.6, 21.4. MALDI-TOF MS (*m/z*): [M]⁺ calculate for C₃₈H₃₀Br₂N₄Zn: 766.73; found: 766.01. FT-IR (ATR) ν/cm⁻¹: 1808, 1604, 1423, 1373, 1315, 1203, 1072, 995, 860, 786, 740, 694, 628, 609.

Synthesis of [5,15-bis-(trimethylsilyl)ethynyl]-10,20-dimesitylporphyrinato] zinc (II) (2). In a schlenk tube under an argon atmosphere, a solution of [5,15-dibromo-10,20-dimesitylporphyrinato] zinc (II) (1.4 mmol, 1.10 g) in 62 mL of THF and 3 mL of Et₃N was added over a mixture of Pd(PPh₃)₂Cl₂ (0.1 mmol, 54 mg) and CuI (0.07 mmol, 13 mg). Afterwards, trimethylsilylacetylene (5.4 mmol, 0.8 mL) was added. The mixture was stirred 18 h. The solvent was removed by rotary evaporation and the solid was purified by column chromatography (silica gel, hexane-CHCl₃, 7:3) and recrystallized from CH₂Cl₂/MeOH. **2** was obtained as a purple solid (1.07 g, 1.35 mmol, 97% yield). ¹H NMR (400 MHz, CDCl₃) δ/ppm: 9.68 (d, 4H, *J* = 4.6 Hz), 8.79 (d, 4H, *J* = 4.6 Hz), 7.33 (s, 4H), 2.68 (s, 6H), 1.86 (s, 12H), 0.62 (s, 18H). ¹³C NMR (100 MHz, CDCl₃) δ/ppm: 152.1, 149.9, 139.0, 138.4, 137.6, 131.9, 131.7, 131.4, 127.7, 120.9, 107.4, 101.5, 100.6, 21.5, 21.5, 0.3. MALDI-TOF MS (*m/z*): [M]⁺ calculated for C₄₈H₄₈N₄Si₂Zn: 800.58; found: 800.27. FT-IR (ATR) ν/cm⁻¹: 2136, 1808, 1604, 1438, 1380, 1334, 1203, 1072, 995, 860, 786, 736, 694, 617.

Synthesis of [5,15-bis-(ethynyl)-10,20-dimesitylporphyrinato] zinc (II). To a solution of **2** (0.7 mmol, 550 mg) in 150 mL of CH₂Cl₂, was added TBAF 1 M in THF (1.65 mmol, 1.65 mL). The solution was stirred at room temperature for 2 h and treated with CaCl₂ (8.2 mmol, 912 mg). The reaction was hydrolyzed with water and extracted with CHCl₃ (3 x 150 mL). The combined organic extract was dried over anhydrous MgSO₄ and filtered; finally, the solvent was removed by rotary evaporation. The deprotected product was quantitatively obtained and it was used in the next synthetic step without further purification.

General Procedure for the Sonogashira coupling reactions. Under an argon atmosphere, a solution of [5,15-bis-(ethynyl)-10,20-dimesitylporphyrinato] zinc (II) (1 eq), the corresponding aldehyde (**3a-b**) (3 eq) and freshly distilled Et₃N (45 mL/mmol) in THF (230 mL/mmol) was added over a mixture of Pd₂(dba)₃ (0.6 eq) and AsPh₃ (3.8 eq). The reaction mixture was refluxed for 18 h. The solvent was removed by rotary evaporation and the solid was purified by column chromatography (silica gel, hexane-CH₂Cl₂, 7:3) followed by recrystallization from CH₂Cl₂/MeOH.

4a: Using the general procedure previously described, [5,15-bis-(ethynyl)-10,20-dimesitylporphyrinato] zinc (II) (0.34 mmol, 658 mg), **3a** (1.02 mmol, 417 mg), 15 mL of Et₃N in 79 mL of THF were allowed to react. **4a** was obtained as a green solid (337 mg, 0.22 mmol, 81% yield). ¹H NMR (400 MHz, CDCl₃) δ/ppm: 9.49 (d, 4H, *J* = 4.4 Hz), 9.16 (s, 2H), 8.75 (d, 4H, *J* = 4.4 Hz), 7.33 (s, 4H), 2.99 (t, 4H, *J* = 7.6 Hz), 2.80 (t, 4H, *J* = 7.6 Hz), 2.69 (s, 6H), 1.89 (s, 12H), 1.60 (t, 4H, *J* = 7.2 Hz), 1.54 (t, 4H, *J* = 7.2 Hz), 1.43–1.22 (m, 24H), 0.93 (t, 6H, *J* = 6.4 Hz), 0.77 (t, 6H, *J* = 7.0 Hz). ¹³C NMR (100 MHz, CDCl₃) δ/ppm: 207.2, 181.2, 151.7, 151.6, 150.1, 148.2, 139.00, 138.1, 137.9, 137.3, 131.9, 131.2, 129.4, 127.8, 122.0, 103.1, 100.1, 89.5, 32.3, 31.8, 31.6, 30.9, 30.9, 29.7, 29.4, 28.7, 27.7, 22.7, 22.6, 21.6, 21.5, 14.1, 14.0. MALDI-TOF MS (*m/z*): [M]⁺ calculated for C₇₆H₈₄N₄O₂S₂Zn: 1212.53; found: 1212.53. FT-IR (ATR) ν/cm⁻¹: 2919, 2854, 2175, 2053, 1650, 1612, 1489, 1438, 1403, 1330, 1284, 1207, 1150, 995, 937, 848, 790, 709.

4b: Using the general procedure previously described, [5,15-bis-(ethynyl)-10,20-dimesitylporphyrinato] zinc (II) (0.34 mmol, 658 mg), **3b** (1.02 mmol, 702 mg), 15 mL of Et₃N in 79 mL of THF. **4b** was obtained as a green solid (246 mg, 0.14, 71%). ¹H NMR (400 MHz, CDCl₃) δ/ppm: 9.56 (s, 1H), 9.55 (d, 4H, *J* = 4.6 Hz), 8.73 (d, 4H, *J* = 4.6 Hz), 7.32 (s, 4H), 7.32 (d, 2H, *J* = 15.5 Hz), 7.08 (d, 2H, *J* = 15.5 Hz), 3.05 (t, 4H, *J* = 7.9 Hz), 2.79 (t, 4H, *J* = 7.9 Hz), 2.75 (t, 4H, *J* = 8.3 Hz), 2.68 (s, 6H), 2.66 (t, 4H, *J* = 7.2 Hz), 1.91 (t, 4H, *J* = 7.2 Hz), 1.89 (s, 12H), 1.67–1.31 (m, 60H), 1.00–0.91 (m, 18H), 0.80 (t, 6H, *J* = 7.2 Hz). ¹³C NMR (100 MHz, CDCl₃) δ/ppm: 181.7, 153.1, 151.6, 149.7, 148.5, 146.9, 142.7, 141.9, 139.0, 138.3, 137.7, 137.3, 134.6, 131.5, 131.1, 127.7, 132.5, 121.5, 119.0, 118.9, 101.2, 100.8, 90.7, 32.2, 31.8,

31.7, 31.6, 31.5, 31.2, 30.9, 29.7, 29.4, 29.3, 29.2, 29.1, 27.5, 27.1, 26.4, 22.7, 22.6, 21.5, 21.4, 14.2, 14.1, 14.0, 13.9. MALDI-TOF MS (m/z): $[M]^+$ calculated for $C_{112}H_{140}N_4O_2S_4Zn$: 1764.92; found: 1765.07. FT-IR (ATR) ν/cm^{-1} : 2919, 2854, 2175, 1646, 1592, 1500, 1454, 1388, 1338, 1292, 1207, 1095, 998, 929, 852, 790, 709.

General procedure for the Knoevenagel condensations. To a solution of **4a-b** (1 eq) in 25 mL/mmol of CH_2Cl_2 , malonitrile (3 eq) and 3 drops of Et_3N were added. The reaction mixture was stirred for 18 h and quenched by the addition of water and extracted with $CHCl_3$ (3 x 150 mL). The combined organic extract was dried over anhydrous $MgSO_4$ and filtered. The solvent was removed by rotary evaporation. The product was purified by column chromatography (silica gel, hexane- CH_2Cl_2 , 1:1) and recrystallized with CH_2Cl_2 : MeOH.

1a: Using the general procedure previously described, **4a** (0.08 mmol, 100 mg) in 2 mL of CH_2Cl_2 were allowed to react with malonitrile (0.25 mmol, 16 mg). **1a** was obtained as a green solid (87 mg, 0.06 mmol, 81% yield). M. p. $>300^\circ C$. 1H NMR (400 MHz, $CDCl_3$) δ/ppm : 9.16 (s, 4H), 8.75 (d, 4H, $J = 4.2$ Hz), 7.89 (s, 2H), 7.37 (s, 4H), 3.84 (m, 4H), 2.76 (m, 4H), 2.71 (s, 6H), 1.96 (s, 12H), 1.76 (m, 4H), 1.64-1.74 (m, 12H), 1.27-1.22 (m, 16H), 0.97 (m, 6H), 0.76 (t, 6H, $J = 6.7$ Hz). ^{13}C NMR (100 MHz, $CDCl_3$) δ/ppm : 154.3, 151.6, 150.3, 147.7, 147.4, 138.9, 138.1, 137.8, 132.2, 131.0, 130.8, 127.9, 122.8, 115.1, 113.9, 106.3, 99.5, 89.4, 75.2, 32.3, 31.7, 31.6, 31.5, 30.9, 30.7, 30.2, 29.7, 29.6, 29.1, 28.8, 22.6, 21.6, 21.5, 14.1, 14.0. MALDI-TOF MS (m/z): $[M]^+$ calculated for $C_{82}H_{84}N_8S_2Zn$: 1308.53; found: 1308.56. FT-IR (ATR) ν/cm^{-1} : 2923, 2854, 2225, 2154, 2053, 1612, 1489, 1465, 1403, 1330, 1288, 1249, 1203, 1083, 998, 937, 850, 790, 711.

1b: Using the general procedure previously described, **4b** (0.2 mmol, 295 mg) in 3 mL of CH_2Cl_2 , malonitrile (0.5 mmol, 33mg). **1b** was obtained as a green solid (246 mg, 0.06 mmol, 79% yield). M. p. $> 300^\circ C$. 1H NMR (400 MHz, $CDCl_3$) δ/ppm : 9.46 (d, 4H, $J = 4.4$ Hz), 8.68 (d, 4H, $J = 4.4$ Hz), 7.69 (s, 2H), 7.28 (s, 4H), 7.21 (d, 2H, $J = 15.6$ Hz), 6.96 (d, 2H, $J = 15.6$ Hz), 2.96 (t, 4H, $J = 7.7$ Hz), 2.70 (t, 4H, $J = 7.7$ Hz), 2.62 (s, 6H), 2.57 (m, 8H), 1.85 (s, 12H), 1.60-1.54 (m, 8H), 1.49-1.26 (m, 56H), 0.94-0.56 (m, 18H), 0.73 (t, 6H, $J = 7.0$ Hz). ^{13}C NMR (100 MHz, $CDCl_3$) δ/ppm : 155.9, 151.6, 149.8, 149.1, 148.8, 147.2, 144.1, 141.6, 139.0, 138.2, 137.8, 137.2, 131.6, 131.1, 128.3, 127.8, 125.7, 120.1, 118.2, 115.6, 114.2, 101.4, 101.2, 90.8, 73.1, 32.2, 31.8, 31.6, 31.6, 31.5, 31.0, 31.9, 29.7, 29.5, 29.3, 29.2, 27.8, 27.5, 26.8, 22.8, 22.7, 22.6, 22.6. MALDI-TOF MS (m/z): $[M]^+$ calculated for $C_{118}H_{140}N_8S_4Zn$: 1860.94; found: 1861.94. FT-IR (ATR) ν/cm^{-1} : 2928, 2856, 2217, 2171, 1552, 1500, 1457, 1399, 1336, 1288, 1209, 1091, 998, 929, 854, 794, 711.

Results and discussion

3.1. Synthesis and Characterizations.

Scheme 1 illustrates the synthetic route used to obtain organic semiconductor compounds **1a** and **1b**, starting from *bis*-trimethylsilyl porphyrin **2**. The trimethylsilyl group was quantitatively removed by hydrolysis with TBAF and, without further purification, reacted with the corresponding iodoaldehyde **3a-b** under Pd-catalyzed Sonogashira coupling conditions to afford the bisaldehydes **4a-b** in 81% and 71% yields, respectively. The ¹H NMR spectra of **4a-b** show the expected signals for both the porphyrin and the thienylenevinylene moieties and the aldehyde protons are observed at 9.16 ppm and 9.56 ppm, respectively. Compound **4b**, only showed the *trans* configuration of the double bond, which was confirmed by a coupling constant of 15.6 Hz. Finally, the target compounds **1a-b** were obtained by Knoevenagel condensations of **4a-b** with malononitrile in the presence of triethylamine in 81% and 79% yields, respectively. In the ¹H NMR spectra of **1a-b**, the aldehyde hydrogen signals are not observed and new vinylic hydrogens signals were observed at 7.89 ppm and 7.69 ppm, respectively, indicating the successful condensation. The mass spectrum of compounds **1a** showed the molecular ion peak at *m/z* 1308.56 amu, while that of compound **1b** exhibited the molecular ion peak at *m/z* 1861.94 amu.

Scheme 1.

Previously, iodoaldehydes **3a-b** were prepared by the reaction of the aldehydes **5a-b**, with molecular iodine (I₂), and bistrifluoroacetoxiodobenzene (PhI(OCOCF₃)₂) in 84% and 62% yield according to Scheme 2.³⁵

Scheme 2.

All compounds were satisfactorily characterized by ¹H and ¹³C NMR, FT-IR and MALDI-MS spectrometry (see the Experimental section and the Supporting Information for synthetic details and full analytical and spectroscopic characterizations).

The thermal stabilities of compounds **1a** and **1b** were evaluated by thermogravimetric analysis (TGA). Compounds **1a-b** display excellent thermal stabilities up to 300 °C with Td of 369 °C and 374 °C for **1a** and **1b**, respectively (Figure S29), which are appropriate for photovoltaic applications.

Optical Properties

The optical properties of **1a** and **1b** in CH₂Cl₂ solutions as well as of their thin-films are shown in Figure 1 and the characteristics of semiconductors **1a** and **1b** are collected in Table 1. The UV-Vis absorption spectra of the precursor aldehydes (**4a-b**) and of the final compounds **1a-b** in solution exhibit a panchromatic absorption in the visible region. These spectra show the Soret band ($\lambda_{\text{max}} = 465$ nm and 499 nm respectively) bathochromically shifted, with respect to the Soret band in the precursor porphyrin **2** ($\lambda_{\text{max}} = 435$ nm, Figure S30). New intense broad bands are observed (at $\lambda_{\text{max}} = 668$ nm for **4a** and 698 nm for **4b**), assigned to intramolecular charge transfer (ICT) (Figure S30). In solution, **1a** and **1b** show absorption ranges from 400 nm to 750 nm with a valley centered at 600 nm. The introduction of the malononitrile fragments (**1a-b**) lead to a bathochromic shift of both bands ($\lambda_{\text{max}} = 499$ and 698 for **1a** and 497 and 705 nm for **1b**) with respect to the corresponding aldehydes (**4a-b**) as a consequence of the extension of the conjugation and due to the strong electron-withdrawing properties of the dicyanomethylene. Increasing the π -conjugation upon increasing the length of the thienylenevinylene in **1b** results in a wider absorbance.

Table 1. UV-Vis,^a Fluorescence Emission^a and OSWV^b data for compounds **1a-b**.

	λ_{max} soln (nm)	log (ϵ)	λ_{max} film (nm)	λ_{em} (nm)	E_{ox}^{d} ^{b, c} (V)	$E_{\text{HOMO}}^{\text{d}}$ (eV)	E_{LUMO} (eV)	E_{0-0}^{e} (eV)
1a	497	5.26	516	717	0.40	-5.50	-3.76	1.75
	705	5.04						
1b	542	5.17	734	747	0.26	-5.36	-3.67	1.69
	731	5.24						

^a 10⁻⁵ M, in dichloromethane; ^b 10⁻³ M in ODCB-acetonitrile (4:1) versus Fc/Fc⁺ ($E_{\text{ox}} = 0.04$ V) glassy carbon, Pt counter electrode, 20 °C, 0.1 M Bu₄NClO₄, scan rate = 100 mV s⁻¹; ^c Nonreversible processes; ^d calculated with respect to ferrocene, E_{HOMO} : -5.1 eV;⁴⁰ ^e estimated from the intersection between the normalized absorption and normalized emission spectra at λ_{max} .

In the solid state, the absorption maximum for **1a** is bathochromically shifted relative to those in solution, by 13 nm. **1b** shows a pronounced absorbance between of 400-850 nm, with a red-shifted maximum of 33 nm (764 nm). These results suggest that the extended backbone in **1b**

results in stronger intermolecular π - π stacking interactions than in **1a** (Figure 2). The estimated optical band gaps were calculated from the thin film absorbance onsets, and were 1.57 eV for **1a** and 1.50 eV for **1b**.

Figure 2.

The fluorescence spectra display a red-shift of the emission band for compound **1b** in comparison to that for **1a**, around 30.2 nm, due to the increased conjugation by one more thienylenevinylene unit. If the emission spectra compounds **1a-b** are compared with those of the precursor aldehydes **4a-b** (Figure S33), a significant quenching of the emission is observed, attributed to more efficient electron transfer processes.

Electrochemical Properties

The electrochemical properties of **1a** and **1b** were investigated using Cyclic Voltammetry (CV) and Osteryoung Square Wave Voltammetry (OSWV) in *o*-DCB-acetonitrile (4:1) (Table 1, Figures 3 and S34). In the anodic scan, both compounds show a first reversible one-electron oxidation wave at 0.40 V for **1a** (Figure 4) and 0.26 V for **1b** (vs Fc/Fc⁺ in all cases) which correspond to the first oxidation of the porphyrin. For **1b**, the extended conjugation gives rise to a decrease of the E_{ox} value by 14 mV with respect to **1a**. A second reversible oxidation wave is observed at 0.78 V for **1a** and at 0.62 V for **1b**. Compound **1b** shows two more non reversible oxidation waves at 0.93 and 1.02 V attributed to the oxidation of the thienylenevinylene moieties. The estimated E_{HOMO} values were calculated with respect to ferrocene as reference (E_{HOMO} : -5.1 eV)⁴⁰ and were determined to be -5.50 eV for **1a** and -5.36 eV for **1b**, in good agreement with the onset oxidation potentials.

Figure 3.

Low-lying HOMO levels should result in high open-circuit voltages (V_{oc}) and are, therefore, desired.⁴¹⁻⁴³ The HOMO-LUMO gaps, optically determined, are as narrow as 1.75 and 1.69 eV for **1a** and **1b**, respectively. The E_{LUMO} of the dyes are higher than that E_{LUMO} of PCBM (-3.9 eV), with values of -3.75 and -3.67 eV for **1a** and **1b**, respectively. Hence, the LUMO energy

levels of these small-molecules match quite well the LUMO energy of PC₆₁BM (-3.9 eV) and PC₇₁BM (-4.0 eV), which suggest an energetically favorable electron transfer from **1a** and **1b** to the acceptor moiety that should in turn favor the exciton dissociation.

Theoretical Calculations

Theoretical calculations were carried out by density functional (DFT) at the B3LYP 6-31G* level *in vacuo* using Gaussian 03W to determine the more stable geometries for both dyes **1a** and **1b** (Figure 4), the HOMO and LUMO energy levels and their molecular orbital contours.

Figure 4.

The optimized structure of both **1a** and **1b**, show that the core is almost perfectly flat, with the aryl groups bounded to the porphyrin core being perpendicular to the macrocycle (dihedral angle of 90°), while the thienylenevinylene fragments are almost in the same plane with respect to the porphyrin rings with a dihedral angle around 0.5°. This planarity allows an extension of the conjugation between the porphyrin and the dicyanovinylene fragments. The bond lengths of the π -conjugated bridge between the porphyrin and the acceptor units are around 1.40 Å, both for single and double bonds, revealing a quinoid character. This fact suggests some zwitterionic contribution to the ground state.

The distribution of the orbital coefficients of the HOMO and LUMO states (Figure 5) show that the charge density of the HOMO of **1a** and **1b** is delocalized over the whole conjugated system, the porphyrin and thienylenevinylene moieties. Similar to the HOMO, the LUMO spreads over the π -conjugated system. Since both orbitals, HOMO and LUMO (Figure 5) are somewhat overlapped, this favors the HOMO to LUMO electronic transitions.

The theoretical HOMO-LUMO gaps are similar for both dyes, being slightly lower for compound **1b** ($\Delta E = 1.72$ eV) than for **1a** ($\Delta E = 1.87$ eV). This fact is mainly due to the more extended conjugation, increasing the HOMO level in **1b** and is related to the bathochromic shift of the maximum absorption wavelength of compound **1b** with respect to that for dye **1a** (according with the experimental data), which improves the light harvesting behaviour. Finally, the offset between the LUMO of the donor (**1a** or **1b**) and the LUMO of the acceptor (PC₆₁BM or PC₇₁BM),⁴¹ from 0.54 eV to 1.01 eV, ensures efficient exciton dissociation at the D/A interface.

Figure 5.**Photovoltaic properties**

To explore the potential photovoltaic (PV) properties of **1a** and **1b**, solar cells were fabricated using the conventional sandwich structure of ITO/poly(3,4-ethylenedioxythiophene):polystyrenesulfonate (PEDOT:PSS)/small molecule: acceptor/Ca/Al. The active layer was spin-coated from chlorobenzene solutions. The ratio of **1a** and **1b** to PC₆₁BM was adjusted, ranging from 1:1 to 1:4 (w/w), and the optimized value was found to be 1:2 for both of them. The optimized ratio was employed in a blend of **1a** and **1b** with PC₇₁BM. The photovoltaic devices were measured under an ambient atmosphere employing AM 1.5G simulated illumination at an intensity of 100 mW/cm². The current density-voltage (*J-V*) characteristics and the external quantum efficiency (EQE) for the conventional device are shown in Figures 6a–d and the performance parameters are summarized in Table 2 as a function of the weight ratios of Donor:PC₆₁BM.

Figure 6.

Figure 6b and Figure 6d illustrate the best photovoltaic performances at varying D/A ratios. Photovoltaic devices containing **1a**:PC₆₁BM exhibited high V_{oc} (0.86 V) at the optimized blend ratio of 1:2 w/w, with a short circuit current (J_{sc}) of 5.72 mA cm⁻², and a fill factor (FF) of 28.4% for an average PCE of 1.45%. Increasing as well as decreasing the amount of PC₆₁BM resulted in a lower PCE. In contrast, photovoltaic devices incorporating a blend of **1b** and PC₆₁BM exhibited an average PCE of 2.70%, with a V_{oc} of 0.82 V, FF of 35.2% and a noteworthy J_{sc} of 9.79 mA cm⁻², because of its more efficient light absorbing properties. Average values were taken from 12 devices. The high values observed for the V_{oc} using **1a** are in agreement with the deeper HOMO level of **1a** (-5.50 eV) vs **1b** (-5.36 eV). The electron acceptor (PC₆₁BM) was replaced by PC₇₁BM due to the broader absorbance and the higher extinction coefficient of the latter in the visible range. SMBHJ devices were fabricated with an architecture of ITO/PEDOT:PSS/**1b** or **1a**:PC₇₁BM (1:2 w/w)/Ca/Al. Photovoltaic devices based on **1b** and PC₇₁BM yielded an increased PCE of 3.21%, a remarkable 14% improvement, with an average J_{sc} of 10.83 mA cm⁻², V_{oc} of 0.82 V and a slightly improved FF (Figure 7). Surprisingly, no improvement was observed employing **1a**:PC₇₁BM (1:2 w/w) as the photoactive layer (see Figure S36). In order to support the performances of the above devices, incident photo-to-current efficiency (IPCE) measurements were also conducted. As shown in Figure 6b, the IPCE response of **1a** with PC₆₁BM covers the visible spectrum ranging, from 300 nm to 800 nm, which matches the absorption spectra. The devices incorporating **1b** exhibited

more efficient photoconversion efficiency than those based on **1a**, due to broader and higher IPCE response in the 300-600 nm range. Therefore, the addition of an extra unit of thienylenevinylene leads to a stronger light-harvesting small-molecule which results in a significant improvement in the power conversion efficiency. In addition, the IPCE values were further improved for a **1b**:PC₇₁BM blend with a remarkable IPCE of 60% at 427 nm (Figure 7). The theoretical J_{sc} values integrated from the EQEs are in good agreement with those experimentally observed in all cases ($\pm 5\%$ mismatch).

Table 2. Summary of the photovoltaic performance of **1a** and **1b** blended with PC₆₁BM and PC₇₁BM under the illumination of AM1.5G, 100 mW/cm².

Active layer	V_{oc} (V)	J_{sc} (mA cm ⁻²)	FF (%)	PCE [Highest] (%)
1a :PC ₆₁ BM (1:4)	0.78 \pm 0.03	5.38 \pm 0.33	27.8 \pm 0.27	1.16 \pm 0.1 [1.26]
1a :PC ₆₁ BM (1:2)	0.86 \pm 0.01	5.67 \pm 0.12	28.1 \pm 0.22	1.36 \pm 0.1 [1.48]
1a :PC ₆₁ BM (1:1)	0.63 \pm 0.02	4.62 \pm 0.13	29.1 \pm 0.21	0.84 \pm 0.1 [0.91]
1b :PC ₆₁ BM (1:4)	0.79 \pm 0.03	8.41 \pm 0.21	33.2 \pm 0.29	2.21 \pm 0.1 [2.34]
1b :PC ₆₁ BM (1:2)	0.82 \pm 0.02	9.44 \pm 0.26	35.0 \pm 0.22	2.70 \pm 0.1 [2.82]
1b :PC ₆₁ BM (1:1)	0.84 \pm 0.02	5.84 \pm 0.30	27.3 \pm 0.21	1.35 \pm 0.1 [1.48]
1a :PC ₇₁ BM (1:2)	0.84 \pm 0.01	5.56 \pm 0.12	26.4 \pm 0.20	1.24 \pm 0.1 [1.34]
1b :PC ₇₁ BM (1:2)	0.82 \pm 0.01	10.83 \pm 0.24	35.7 \pm 0.24	3.16 \pm 0.1 [3.21]

Figure 7.

Inspecting the morphology of the photoactive layers by atomic force microscopy using the tapping mode (AFM) provided some explanation for lower power conversion efficiencies obtained for the photovoltaic devices⁴⁴ incorporating **1a** and **1b** when blended with PC₆₁BM and PC₇₁BM (Figure 8). The topography images for PC₆₁BM and PC₇₁BM reveal the formation of coarse morphologies with faceted islands features showing a root-mean-square roughness (rms) of 1.9 and 1.7 nm, respectively. Large aggregates of several hundred nanometers were observed which limit the exciton dissociation efficiencies and the charge transport, explaining the lower FF and J_{sc} values measured for these devices. On the other hand, the surface morphology of devices containing **1b**:PC₆₁BM and **1b**:PC₇₁BM exhibit a smoother surface topography (rms of 1.0 and 0.9 nm, respectively) with smaller aggregate sizes indicating better morphological features for exciton dissociation at the donor-acceptor interfaces, which correlate with the higher FF and J_{sc} and higher power conversion efficiencies observed.

Figure 8.**Conclusions**

In conclusion, we have synthesized two new conjugated acceptor-donor-acceptor (A- π -D- π -A) compounds having a Zn-porphyrin acting as donor and linked by ethynylenes to one or two units of thienylenevinylene and capped by dicyanovinylene groups as acceptor units. Incorporation of electron-accepting dicyanovinylene moieties through the thiophene based bridges shift the absorption profiles bathochromically to the NIR due to an intense intramolecular charge transfer band. **1a** and **1b** exhibit not only excellent light harvesting properties but also thermal stability and low-lying HOMO levels at -5.50 and -5.36 eV. Photovoltaic devices incorporating **1b** blended with PC₇₁BM displayed a moderate PCE of 3.21% compared to that of **1a** (PCE of 1.4%). Extension of the conjugation in **1b** results in a significantly much higher J_{sc} and FF compared to that of **1a**. In order to chase higher efficiencies, further variations in the molecular structure are currently underway in our laboratories.

Acknowledgements

Financial support from the Ministry of Science and Innovation of Spain, (CTQ2013-48252-P) and Junta de Comunidades de Castilla-La Mancha (PEII-2014-014-P) is gratefully acknowledged. SA thanks to the Fundación Carolina for a grant. LE wishes to thank the Robert A. Welch Foundation for an endowed chair (AH-0033) and the National Science Foundation, grant DMR-1205302 (PREM Program) for generous financial support.

Appendix A. Supplementary data

Supplementary data related to this article can be found at

References

- 1 G. Yu, J. Gao, J. C. Hummelen, F. Wudl and A. J. Heeger, *Science* 1995, **270**, 1789-1791.
- 2 H. Y. Chen, J. H. Hou, S. Q. Zhang, Y. Y. Liang, G. W. Yang, Y. Yang, L. P. Yu, Y. Wu and G. Li, *Nat. Photon.*, 2009, **3**, 649-653.
- 3 G. Li, R. Zhu, and Y. Yang, *Nat. Photon.*, 2012, **6**, 153-161.
- 4 T. Yang, M. Wang, C. Duan, X. Hu, L. Huang, J. Peng, F. Huang and X. Gong, *Energy Environ. Sci.*, 2012, **5**, 8208.

- 5 J. Subbiah, B. Purushothaman, M. Chen, T. Qin, M. Gao, D. Vak, F. H. Scholes, X. Chen, S. E. Watkins, G. J. Wilson, A. B. Holmes, W. W. H. Wong and D. J. Jones, *Adv. Mater.*, 2015, **27**, 702–705.
- 6 T. Ameri, N. Li and C. J. Brabec, *Energy Environ. Sci.*, 2013, **6**, 2390-2413.
- 7 A. Mishra and P. Bäuerle, *Angew. Chem. Int. Ed.*, 2012, **51**, 2020-2067.
- 8 Y. Chen, Y. Wan and G. Long, *Acc. Chem. Res.*, 2013, **46**, 2645-2655.
- 9 A. J. Heeger, *Adv. Mater.*, 2014, **26**, 10-28.
- 10 J. Roncali, P. Leriche and P. Blanchard, *Adv. Mater.*, 2014, **26**, 3821-3838.
- 11 B. Kan, Q. Zhang, M. Li, X. Wan, W. Ni, G. Long, Y. Wang, X. Yang, H. Feng and Y. Chen, *J. Am. Chem. Soc.*, 2014, **136**, 15529-15532.
- 12 Q. Zhang, B. Kan, F. Liu, G. Long, X. Wan, X. Chen, Y. Zuo, W. Ni, H. Zhang, M. Li, Z. Hu, F. Huang, Y. Cao, Z. Liang, M. Zhang, T. P. Russell and Y. Chen, *Nat. Photon.*, 2015, **9**, 35-41.
- 13 J. Zhou, Y. Zuo, X. Wan, G. Long, Q. Zhang, W. Ni, Y. Liu, Z. Li, G. He, C. Li, B. Kan, M. Li and Y. Chen, *J. Am. Chem. Soc.*, 2013, **135**, 8484-8487.
- 14 Y. Sun, G. C. Welch, W. L. Leong, C. J. Takacs, G. C. Bazan and A. J. Heeger, *Nat. Mater.*, 2012, **11**, 44-48.
- 15 Y. Liu, C. Chen, Z. Hong, J. Gao, Y. M. Yang, H. Zhou, L. Dou, G. Li and Y. Yang, *Sci. Rep.*, 2013, **3**, 3356.
- 16 D. Gust, T. A. Moore and A. L. Moore, *Acc. Chem. Res.*, 2009, **42**, 1809-1818
- 17 H. Imahori, T. Umeyama and S. Ito, *Acc. Chem. Res.*, 2001, **34**, 40-48.
- 18 M. V. Martínez-Díaz, G. de la Torre and T. Torres, *Chem. Commun.*, 2010, **46**, 7090-7108.
- 19 L.-L. Li and E. W. Diau, *Chem. Soc. Rev.*, 2013, **42**, 291–304.
- 20 M. K. Panda, K. Ladomenou and A. G. Coutsolelos, *Coord. Chem. Rev.*, 2012, **256**, 2601-2627.
- 21 E. M. Barea, R. Caballero, L. López-Arroyo, A. Guerrero, P. de la Cruz, F. Langa and J. Bisquert, *ChemPhysChem* 2011, **12**, 961-965.
- 22 A. Aljarilla, J. N. Clifford, L. Pelleja, A. Moncho, S. Arrechea, P. de la Cruz, F. Langa and E. Palomares, *J. Mat. Chem. A.*, 2013, **1**, 13640-13647.
- 23 S. Mathew, A. Yella, P. Gao, R. Humphry-Baker, B. F. E. Curchod, N. Ashari-Astani, I. Tavernelli, U. Rothlisberger, Md. K. Nazeeruddin and M. Michael Grätzel, *Nat. Chem.*, 2014, **6**, 242-247.
- 24 Y. Huang, L. Li, X. Peng, J. Peng and Y. Cao, *J. Mater. Chem.*, 2012, **22**, 21841-21844.
- 25 L. Li, Y. Huang, J. Peng, Y. Cao and X. Peng, *J. Mater. Chem. A*, 2013, **1**, 2144-2150.
- 26 H. Qin, L. Li, F. Guo, S. Su, J. Peng, Y. Cao, X. Peng, *Energy Environ. Sci.*, 2014, **7**, 1397-1401.

- 27 Q. Sun, L. Dai, X. Zhou, L. Li and Q. Li, *Appl. Phys. Lett.* 2007, **91**, 253505/1-253505/3.
- 28 T. Oku, T. Noma, A. Suzuki, K. Kikuchi and S. Kikuchi, *J. Phys. Chem. Solids*, 2010, **71**, 551-555.
- 29 J. Hatano, N. Obata, S. Yamaguchi, T. Yasuda and Y. Matsuo, *J. Mat. Chem.*, 2012, **22**, 19258-19263.
- 30 C. V. Kumar, L. Cabau, E. N. Koukaras, G. D. Sharma and E. Palomares, *Nanoscale*, 2015, **7**, 179-189.
- 31 A. Luechai, J. Gasiorowski, A. Petsom, H. Neugebauer, N. S. Sariciftci and P. Thamyongkit, *J. Mater. Chem.*, 2012, **22**, 23030-23037.
- 32 T. Kengthanomma, P. Thamyongkit, J. Gasiorowski, A. M. Ramil and N. S. Sariciftci, *J. Mat. Chem. A*, 2013, **1**, 10524-10531.
- 33 J. Rawson, A. C. Stuart, W. You, and M. J. Therien, *J. Am. Chem. Soc.*, 2014, **136**, 17561-17569.
- 34 C. Y. Chang, Y. J. Cheng, S. H. Hung, J. S. Wu, W. S. Kao, C. H. Lee and C. S. Hsu, *Adv. Mater.*, 2012, **24**, 549-553.
- 35 L. Pellejà, R. Dominguez, A. Aljarilla, J. N. Clifford, P. de la Cruz, F. Langa and E. Palomares, *ChemElectroChem*, 2014, **1**, 7, 1126-1129.
- 36 F. Oswald, D. M. S. Islam, Y. Araki, V. Troiani, P. de la Cruz, A. Moreno, O. Ito and F. Langa, *Chem. Eur. J.*, 2007, **13**, 3924-3933.
- 37 L. Yu, K. Muthukumar, I. V. Sazanovich, C. Kirmaier, E. Hindin, J. R. Diers, P. D. Boyle, D. F. Bocian, D. Holten and J. S. Lindsey, *Inorg. Chem.*, 2003, **42**, 6629-6647.
- 38 K. L. Joydev, S. Dhanalekshmi, M. Taniguchi, A. Ambroise and J. S. Lindsey, *Org. Proc. Res. Dev.* 2003, **7**, 799-812.
- 39 B. Jiang, S. W. Yang, D. C. Barbini and W. E. Jr. Jones, *Chem. Commun.*, 1998, 213-214.
- 40 C. M. Cardona, W. Li, A. E. Kaifer, D. Stockdale and G. C. Bazan, *Adv. Mater.*, 2011, **23**, 2367-2371.
- 41 A. Cravino, *Appl. Phys. Lett.*, 2007, **91**, 243502.
- 42 G. Dennler, M. C. Scharber and C. J. Brabec, *Adv. Mater.*, 2009, **21**, 1323-1338.
- 43 M. C. Scharber, D. Mühlbacher, M. Koppe, P. Denk, C. Waldauf, A. J. Heeger and C. J. Brabec, *Adv. Mater.*, 2006, **18**, 789-794.
- 44 Y. Huang, E. J. Kramer, A. J. Heeger and G. C. Bazan, *Chem. Rev.* 2014, **114**, 7006-7043.

Figure 1. Structures of **1a** and **1b**.

Scheme 1. Synthetic route to chromophores **1a** and **1b**.

Scheme 2. Synthesis of precursor aldehydes **3a,b**.

Figure 2. Normalized UV-Vis spectra of **1a** (a) and **1b** (b) in DCM solution (black line) and in thin films (red line).

Figure 3. CV plot of compound **1a**.

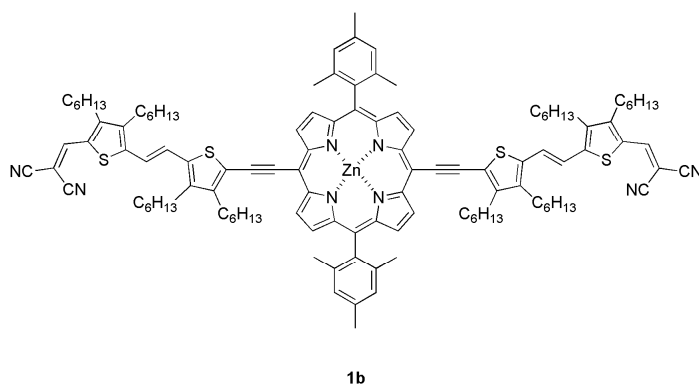
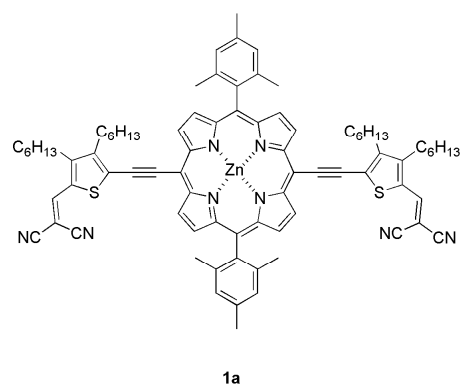
Figure 4. Optimized geometries of dyes **1a** and **1b**.

Figure 5. Electronic density contours and energy levels for HOMO-1, HOMO, LUMO, and LUMO+1 calculated at the B3LYP/6-31G** level for dyes **1a** and **1b** compared with the energy levels of the PC₆₁BM and PC₇₁BM frontier orbitals.

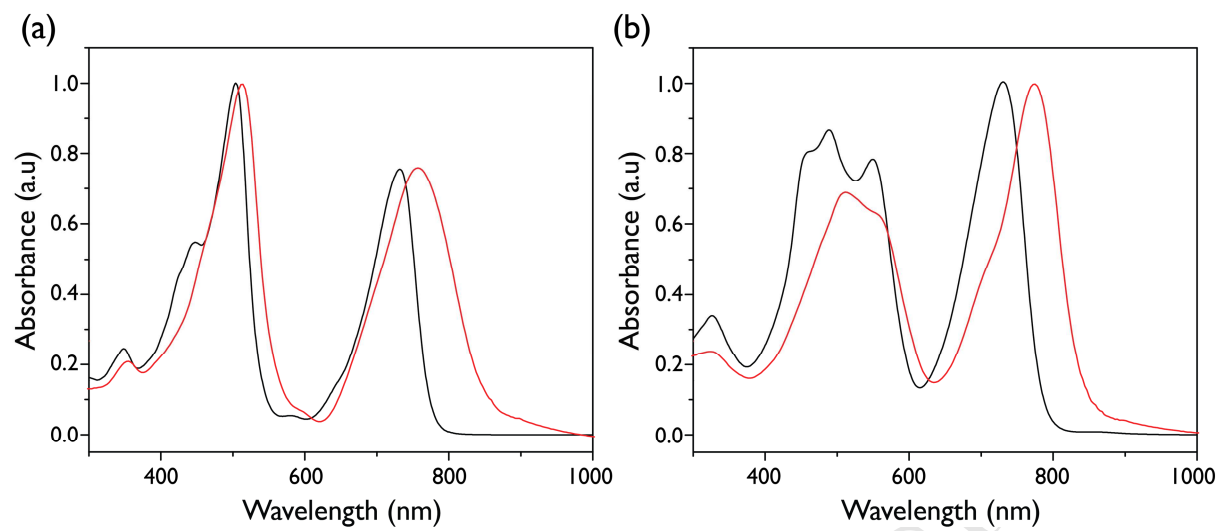
Figure 6. EQE and *J-V* characteristics of the SMBHJ for **1a** and **1b** blending with PC₆₁BM at different ratios.

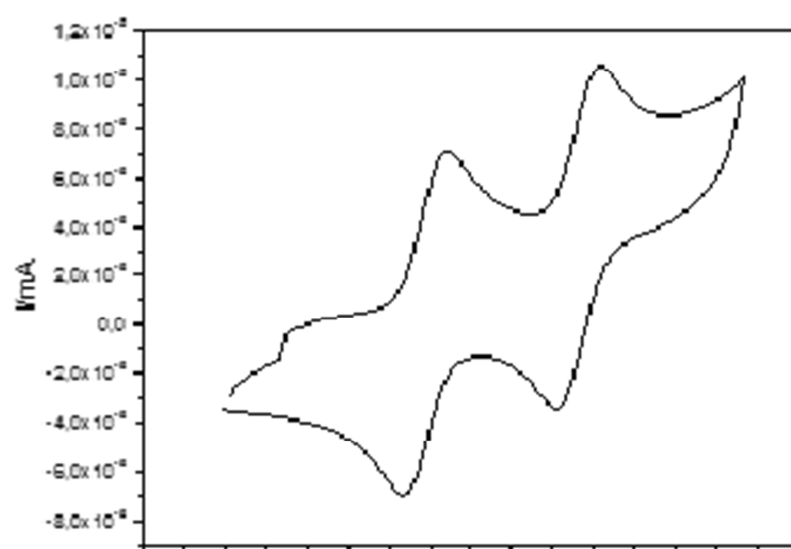
Figure 7. EQE (a) and *J-V* (b) characteristics of the SMBHJ for **1b** blending with PC₆₁BM and PC₇₁BM in a 1:2 ratio.

Figure 8. Tapping mode AFM height images (2 μm x 2 μm) of **1a** films spin-coated from chlorobenzene blended with (a) PC₆₁BM and (b) PC₇₁BM; Tapping mode AFM height images (2 μm x 2 μm) of **1b** films spin-coated from chlorobenzene blended with (c) PC₆₁BM and (d) PC₇₁BM.

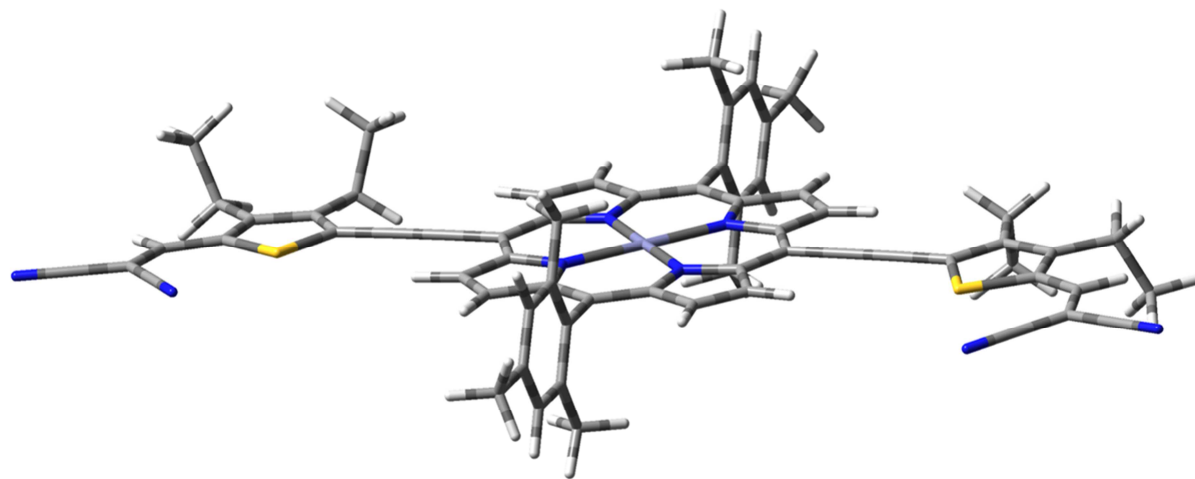


ACCEPTED MANUSCRIPT

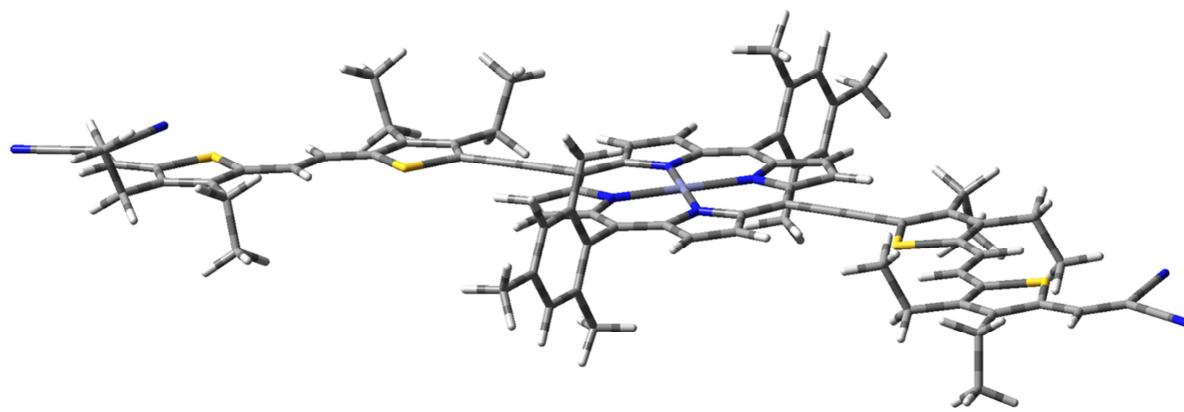




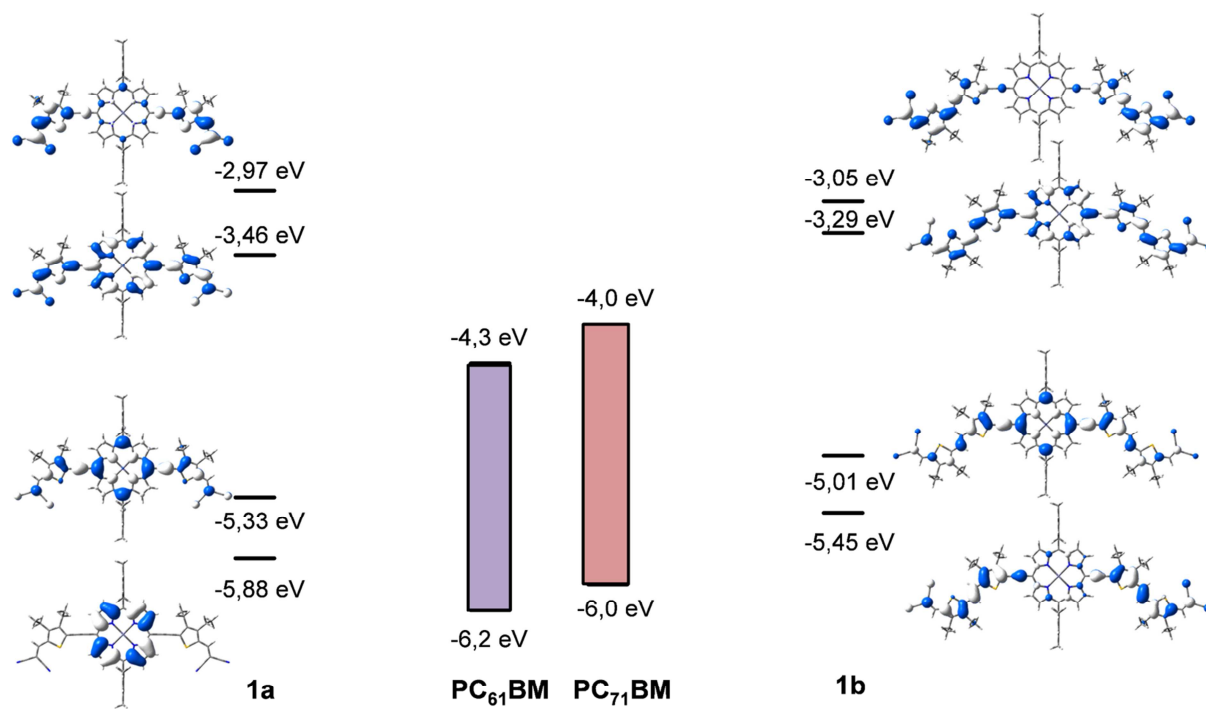
ACCEPTED MANUSCRIPT

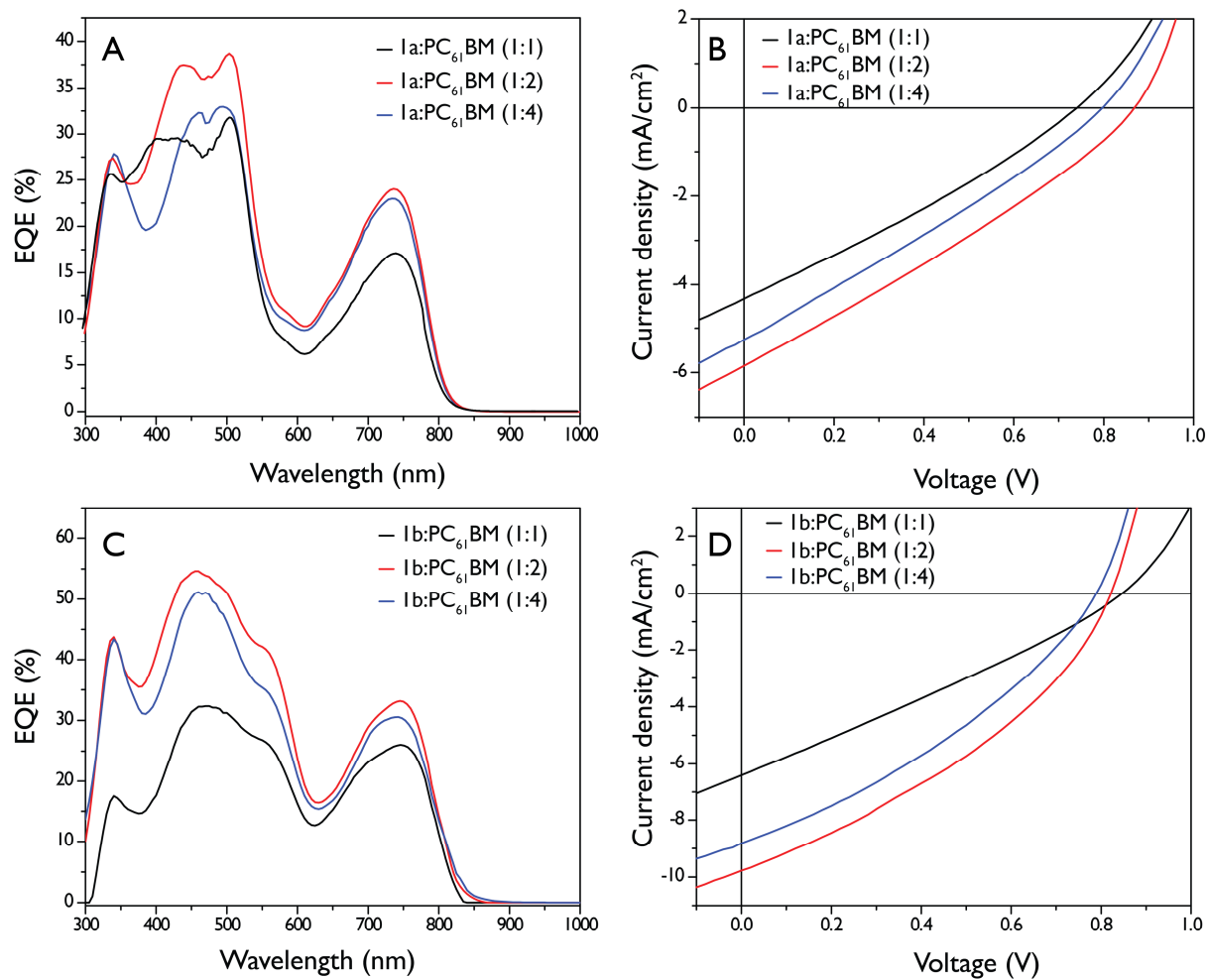


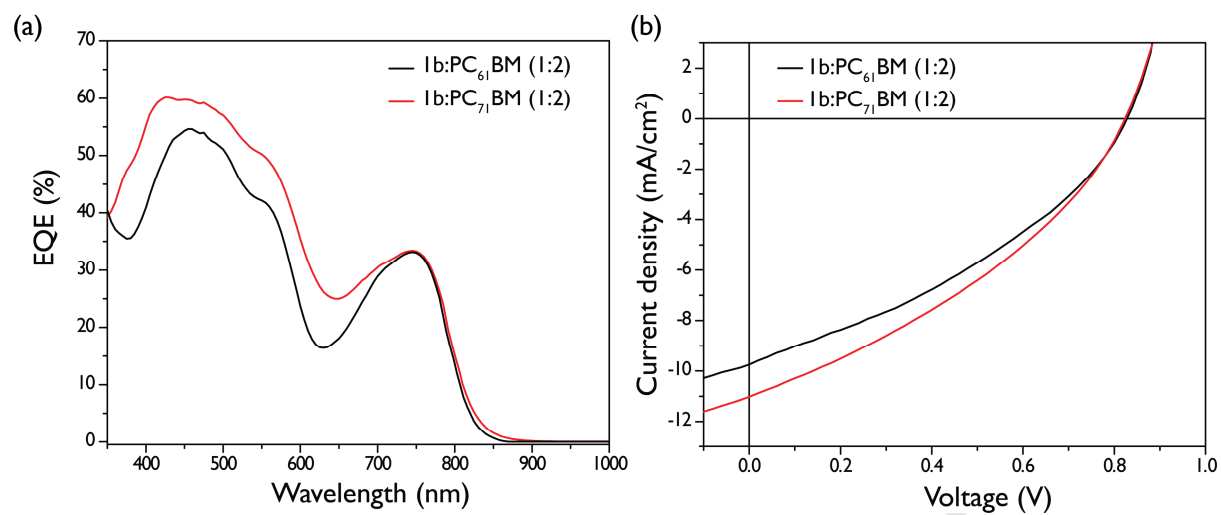
ACCEPTED MANUSCRIPT

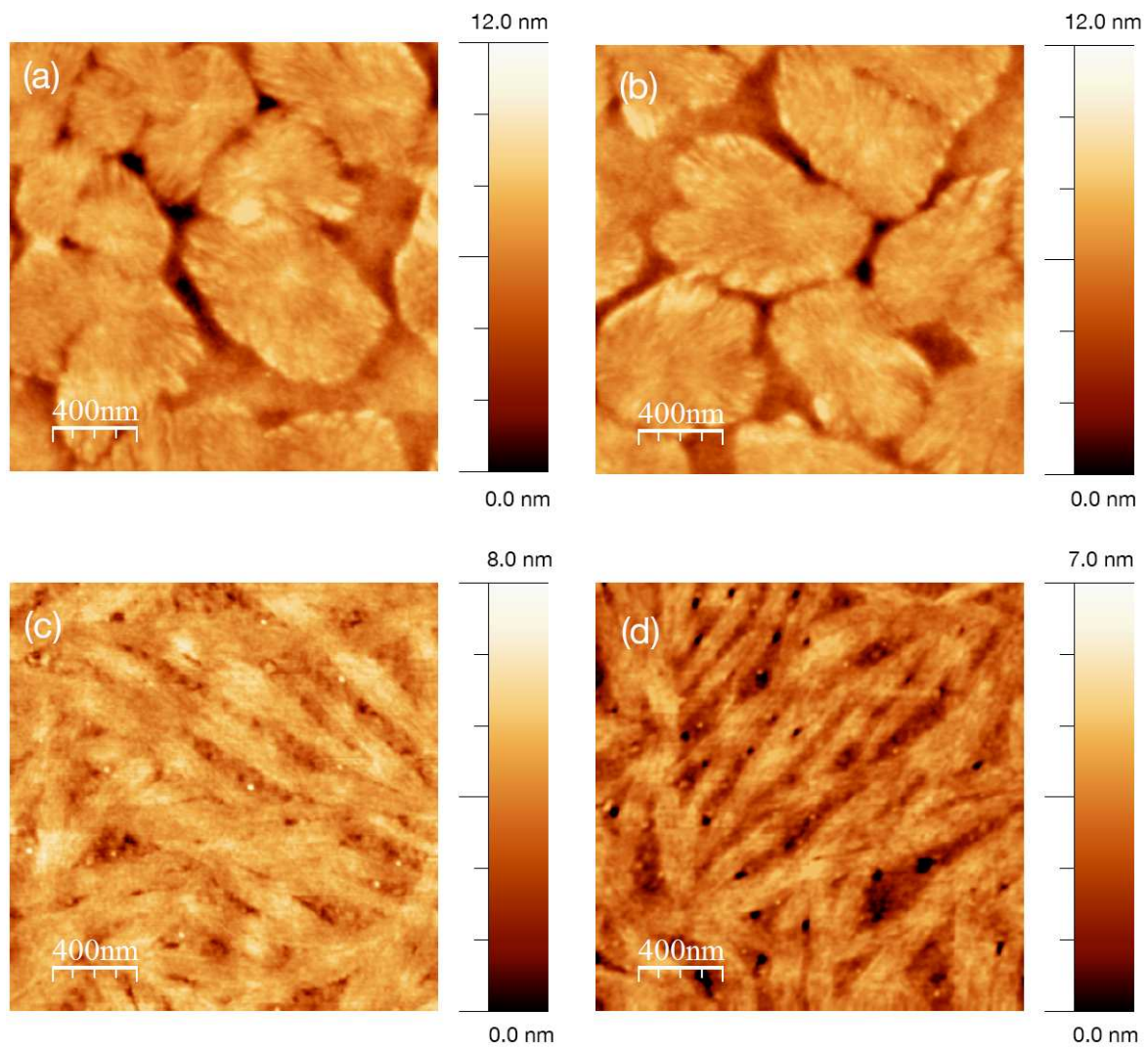


ACCEPTED MANUSCRIPT

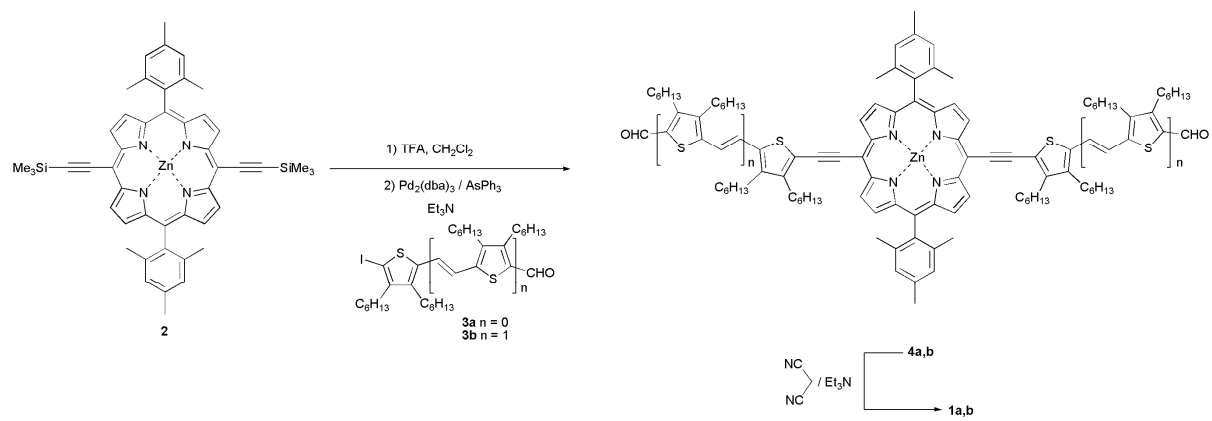


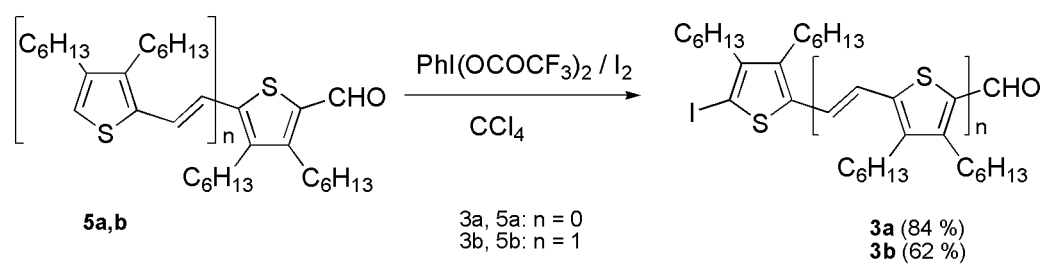






ACCEPTED





ACCEPTED MANUSCRIPT

- The molecules **1a** and **1b** exhibit excellent light harvesting properties, thermal stability and low-lying HOMO levels.
- Photovoltaic devices incorporating **1b** blended with PC₇₁BM displayed a moderate PCE of 3.21% compared to that of **1a** (PCE of 1.4%).
- Extension of the conjugation in **1b** results in a significantly much higher J_{sc} and FF compared to that of **1a**.

New Acceptor- π -Porphyrin- π -Acceptor Systems for Solution-Processed Small Molecule Organic Solar Cells

Susana Arrechea,^a Agustín Molina-Ontoria,^b Ana Aljarilla,^a Pilar de la Cruz,^a
Fernando Langa^{a,*} and Luis Echegoyen^{b,*}

^a *Universidad de Castilla-La Mancha. Institute of Nanoscience, Nanotechnology and Molecular Materials (INAMOL), Campus de la Fábrica de Armas, Toledo, Spain; Fax: 34 9252 68840; Tel: 34 9252 68843; E-mail: Fernando.Langa@uclm.es*

^b *Department of Chemistry, University of Texas at El Paso, El Paso, TX 79968, USA.; Tel: 915-747-7573; E-mail: echegoyen@utep.edu*

Table of contents

1. Experimental details	S2
2. ¹ H-NMR, ¹³ C-NMR, FT-IR and MALDI-TOF o MS spectra	S5
3. Thermogravimetric analysis	S21
4. UV-Visible and emission spectroscopies	S22
5. Square Wave plots	S24
6. EQE and IV characteristic for 1a:PC71BM (1:2)	S26

1. Experimental details

Synthetic procedures were carried out under inert argon atmosphere, in dry solvent unless otherwise noted. All reagents and solvents were reagent grade and were used without further purification. Chromatographic purifications were performed using silica gel 60 SDS (particle size 0.040-0.063 mm). Analytical thin-layer chromatography was performed using Merck TLC silica gel 60 F254. ¹H-NMR spectra were obtained on Bruker TopSpin AV-400 (400 MHz) spectrometer. Chemical shifts are reported in parts per million (ppm) relative to the solvent residual peak (CDCl₃, 7.27 ppm). ¹³C-NMR chemical shifts (δ) are reported relative to the solvent residual peak (CDCl₃, 77.0 ppm). UV-Vis measurements were carried out on a Shimadzu UV 3600 spectrophotometer. For extinction coefficient determination, solutions of different concentration were prepared in CH₂Cl₂ (HPLC grade) with absorption between 0.1-1 of absorbance using a 1 cm UV cuvette. The emission measurements were carried out on Cary Eclipse fluorescence spectrophotometer. Mass spectra (MALDI-TOF) were recorded on a VOYAGER DETM STR mass spectrometer using dithranol as matrix. Melting points are uncorrected.

The molecular geometries and frontier molecular orbitals of these new dyes have been optimized by density functional theory (DFT) calculations at the B3LYP/6-31G* level.¹

¹ Gaussian 03, Revision D.02, Frisch, M. J.; Trucks, G. W.; Schlegel, H. B.; Scuseria, G. E.; Robb, M. A.; Cheeseman, J. R.; Montgomery Jr., J. A.; Vreven, T.; Kudin, K. N.; Burant, J. C.; Millam, J. M.; Iyengar, S. S.; Tomasi, J.; Barone, V.; Mennucci, B.; Cossi, M.; Scalmani, G.; Rega, N.; Petersson, G. A.; Nakatsuji, H.; Hada, M.; Ehara, M.; Toyota, K.; Fukuda, R.; Hasegawa, J.; Ishida, M.; Nakajima, T.; Honda, Y.; Kitao, O.; Nakai, H.; Klene, M.; Li, X.; Knox, J. E.; Hratchian, H. P.; Cross, J. B.; Bakken, V.; Adamo, C.; Jaramillo, J.; Gomperts, R.; Stratmann, R. E.; Yazyev, O.; Austin, A. J.; Cammi, R.; Pomelli, C.; Ochterski, J. W.; Ayala, P. Y.; Morokuma, K.; Voth, G. A.; Salvador, P.; Dannenberg, J. J.; Zakrzewski, V. G.; Dapprich, S.; Daniels, A. D.; Strain, M. C.; Farkas, O.; Malick, D. K.; Rabuck, A. D.; Raghavachari, K.; Foresman, J. B.; Ortiz, J. V.; Cui, Q.; Baboul, A. G.; Clifford, S.; Cioslowski, J.; Stefanov, B. B.; Liu, G.; Liashenko, A.; Piskorz, P.; Komaromi, I.; Martin, R. L.; Fox, D. J.; Keith, T.; Al-Laham, M. A.; Peng, C. Y.; Nanayakkara, A.; Challacombe, M.; Gill, P. M. W.;

Cyclic voltammetry was performed in ODCB-acetonitrile (4:1) solutions. Tetrabutylammonium perchlorate (0.1 M as supporting electrolyte) were purchased from Acros and used without purification. Solutions were deoxygenated by argon bubbling prior to each experiment which was run under argon atmosphere. Experiments were done in a one-compartment cell equipped with a platinum working microelectrode ($\varnothing = 2$ mm) and a platinum wire counter electrode. An Ag/AgNO₃ (0.01 M in CH₃CN) electrode was used as reference and checked against the ferrocene/ferrocenium couple (Fc/Fc⁺) before and after each experiment.

The thermal stability was evaluated by TGA on a Mettler Toledo TGA/DSC Start^e System under nitrogen, with a heating rate of 10 °C/min. Heating of crystalline samples leads to melting of the solids, but no recrystallization was observed.

SM BHJ device preparation

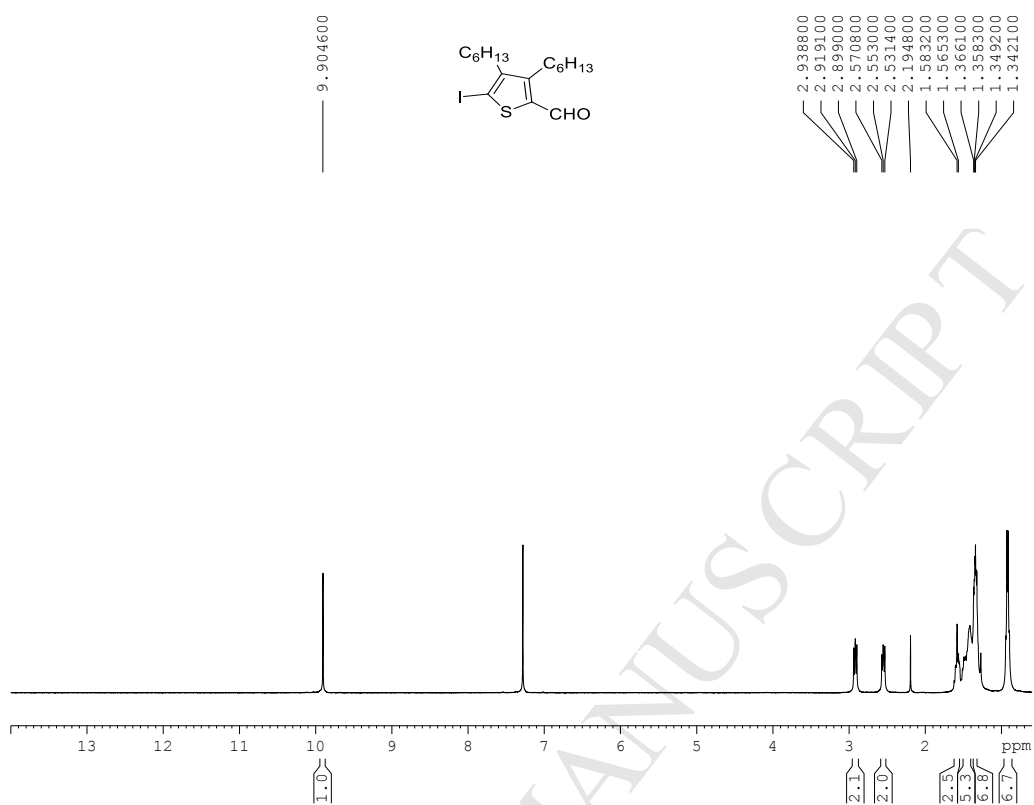
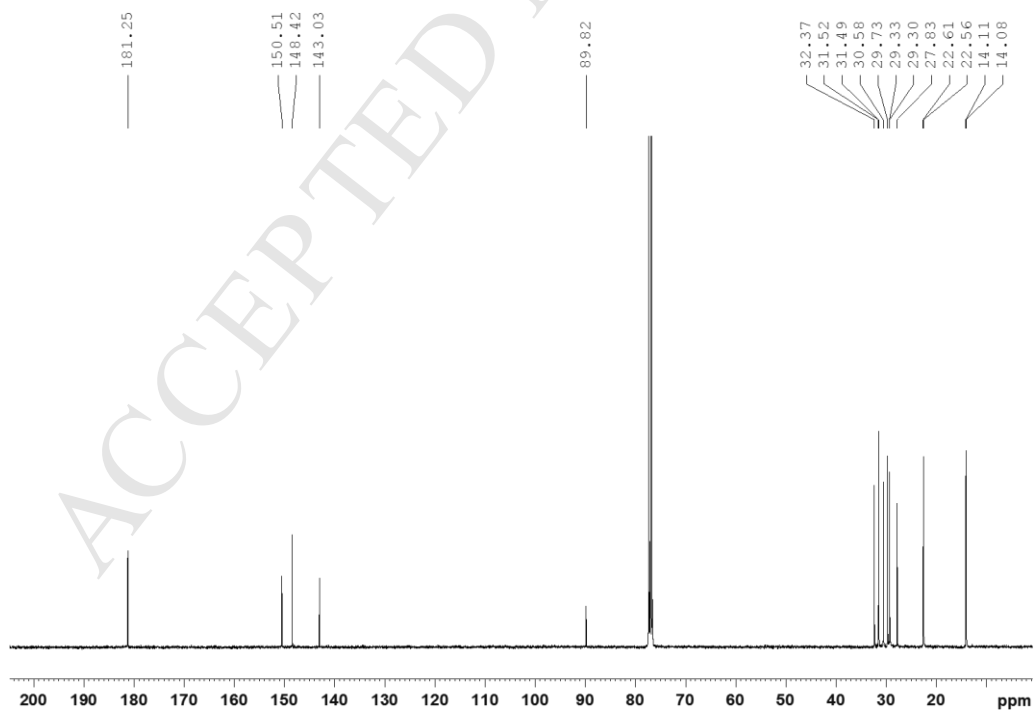
PC₆₁BM and PC₇₁BM were purchased from American Dye Source and used as received.

The ITO-coated glasses (Delta technologies, 5-15 Ω) were pre-cleaned stepwise by ultracentrifugation 15 minutes in detergent, deionized water, methanol, acetone and iso-propanol and then by a 30 minutes UV-ozone treatment. A thin layer of PEDOT:PSS (Clevios P VP AI 4083, 5000 rpm, 30 seconds, ≈ 30 nm) was spin-coated onto the ITO and baked at 150 °C for 15 minutes in air. Subsequently, the active layer (**1a-b**:PC₆₁BM, 30 mg/mL) with varying weight ratios (1:4, 1:2 and 1:1) was spin-coated at 1500 rpm from chlorobenzene solutions. **1a** or **1b**, **1a-b**:PC₇₁BM (1:2, 30 mg/mL) was spin-coated at 1500 rpm. Then the devices were transferred to a N₂ filled glove box (<0.1 ppm O₂ and < 0.1 ppm H₂O) for further processing. The photoactive layer was annealed at 80 °C for 10 minutes followed by thermal evaporation of 20 nm of calcium and 80 nm of aluminum (1×10^{-6} mbar) with a shadow mask of 0.4 cm². The photovoltaic properties were measured under 1 sun, AM1.5G (air mass 1.5 global) spectrum from a solar simulator (Photo

Johnson, B.; Chen, W.; Wong, M. W.; Gonzalez, C.; Pople, J. A. Gaussian, Inc., Wallingford CT, 2004.

Emission Tech CT100) at 100 mW/cm²). The J_{sc} - V_{oc} characteristics were recorded with a Keithley 2420 source unit.

ACCEPTED MANUSCRIPT

2. ^1H NMR, ^{13}C NMR, FT-IR and MALDI-TOF MS spectraFigure S1. ^1H NMR spectrum (400 MHz, CDCl_3) of **3a**.Figure S2. ^{13}C NMR spectrum (100 MHz, CDCl_3) of **3a**.

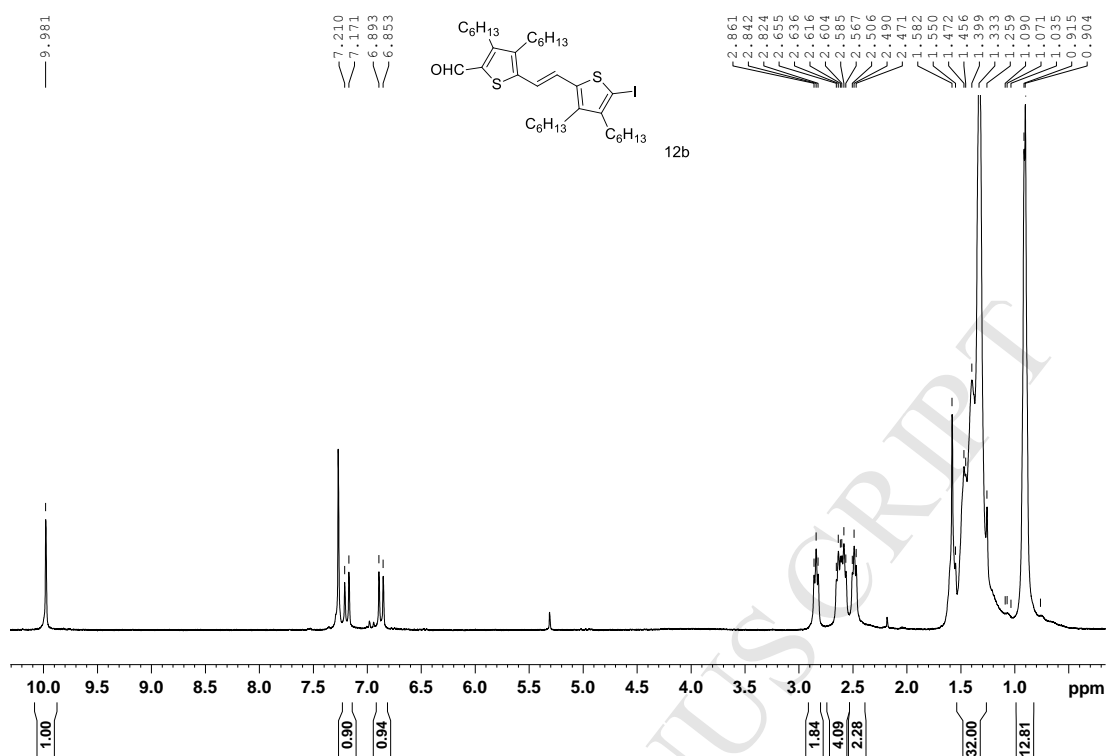


Figure S3. ^1H NMR spectrum (400 MHz, CDCl_3) of **3b**.

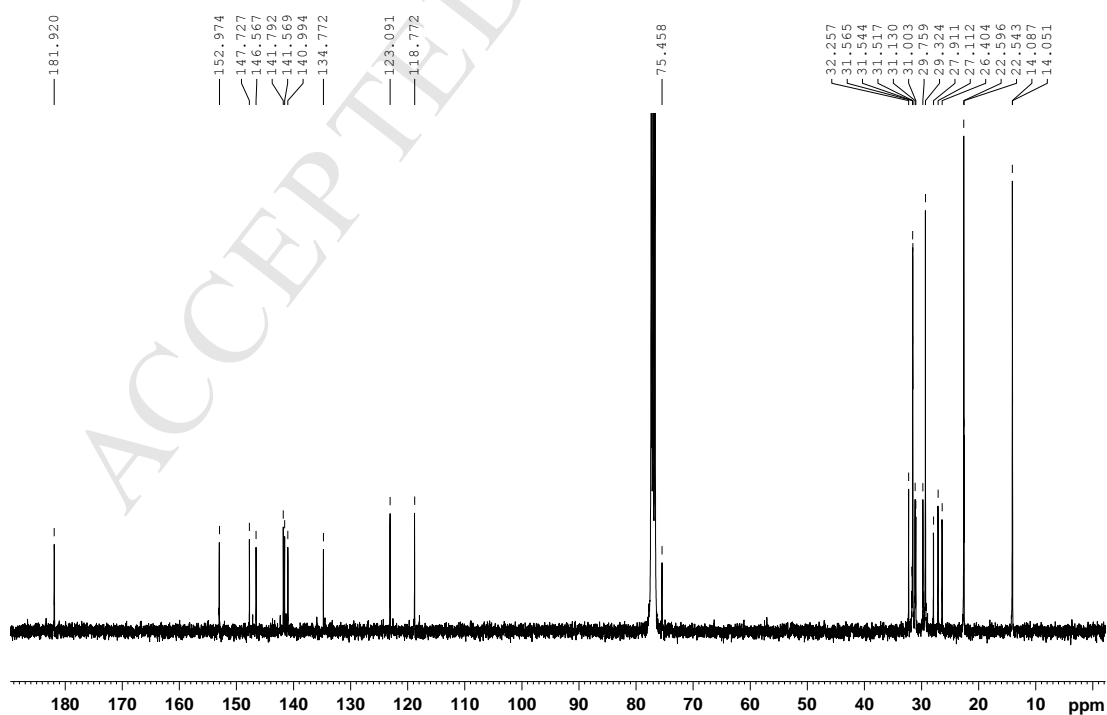


Figure S4. ^{13}C NMR spectrum (100 MHz, CDCl_3) of **3b**.

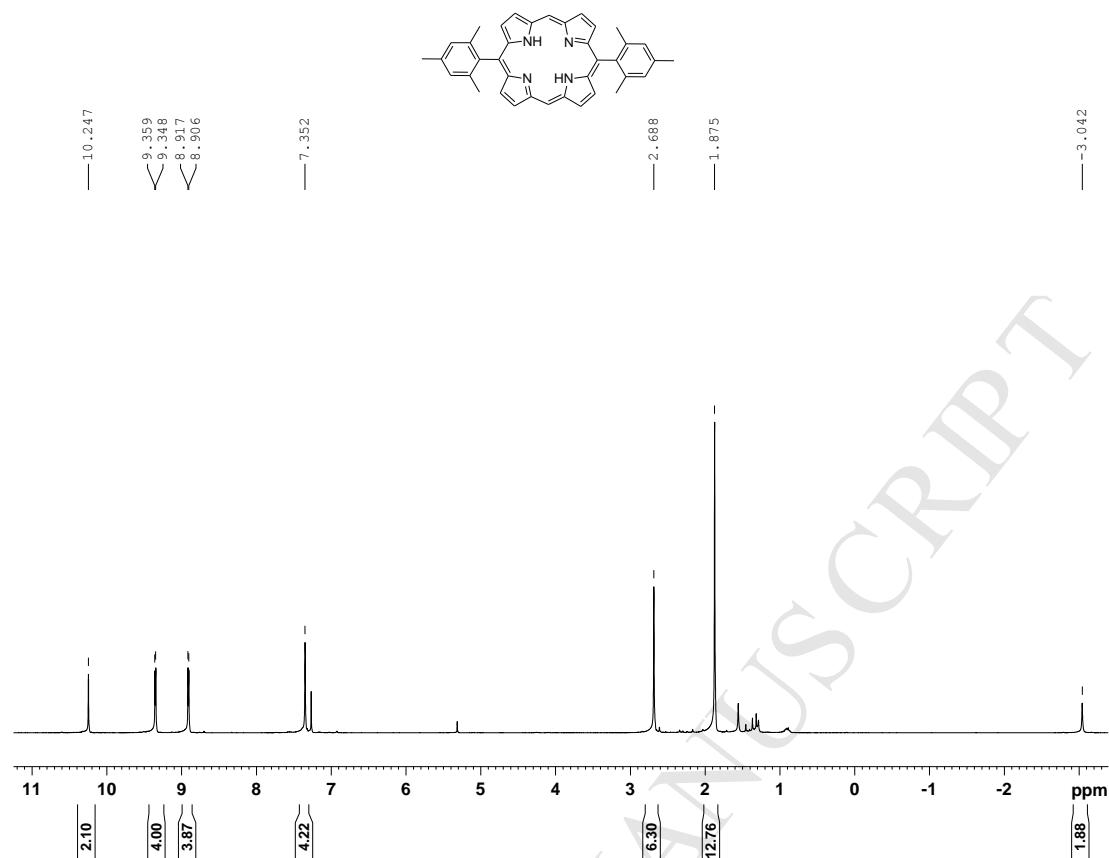


Figure S5. ¹H NMR spectrum (400 MHz, CDCl₃) of 5,15-Dimesitylporphyrin.

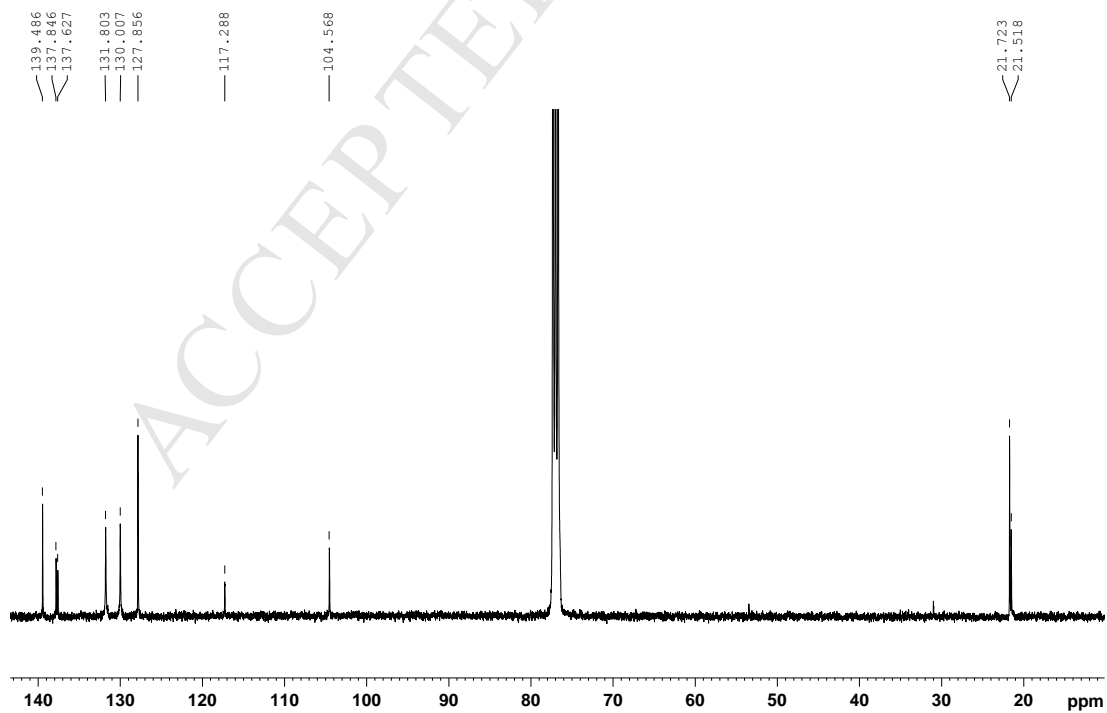


Figure S6. ¹³C NMR spectrum (100 MHz, CDCl₃) of 5,15-Dimesitylporphyrin.

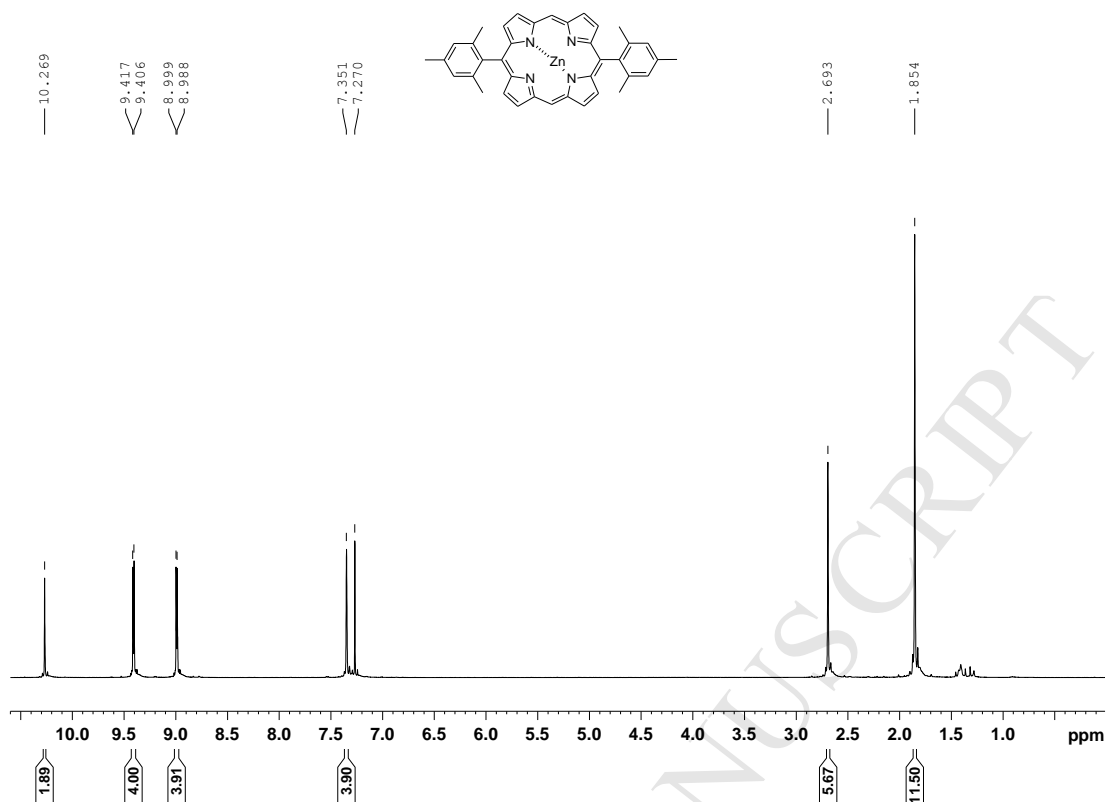


Figure S7. ¹H NMR spectrum (400 MHz, CDCl₃) of [5,15-Dimesitylporphyrinato] zinc (II).

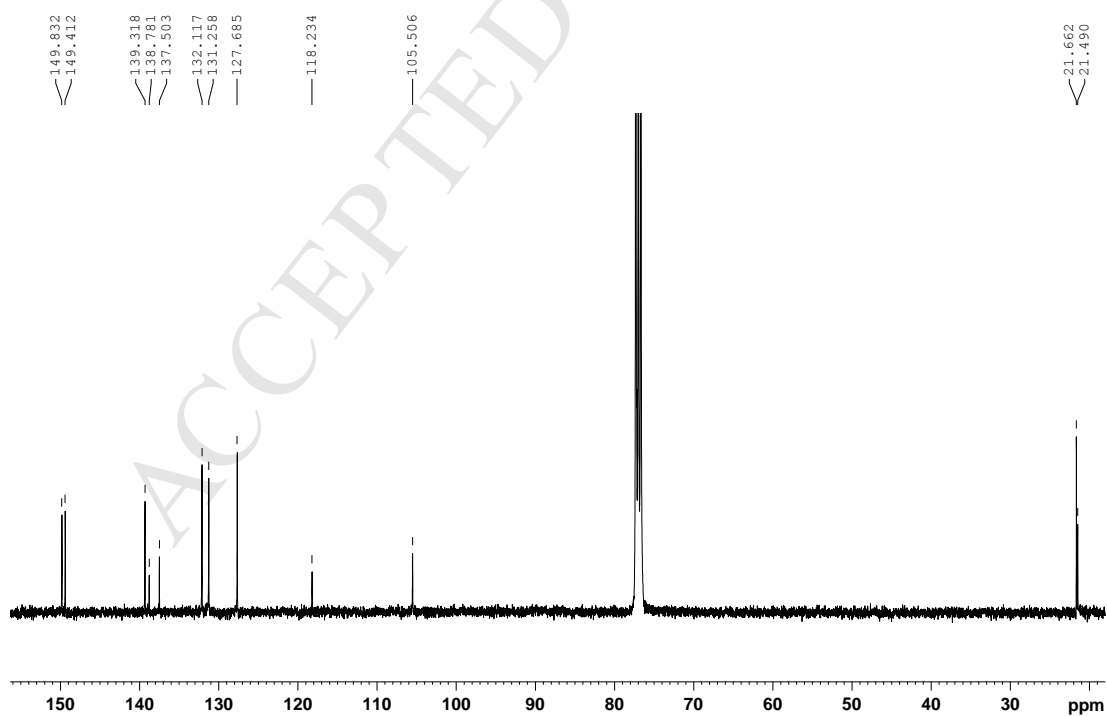


Figure S8. ¹³C NMR spectrum (100 MHz, CDCl₃) of [5,15-Dimesitylporphyrinato] zinc (II).

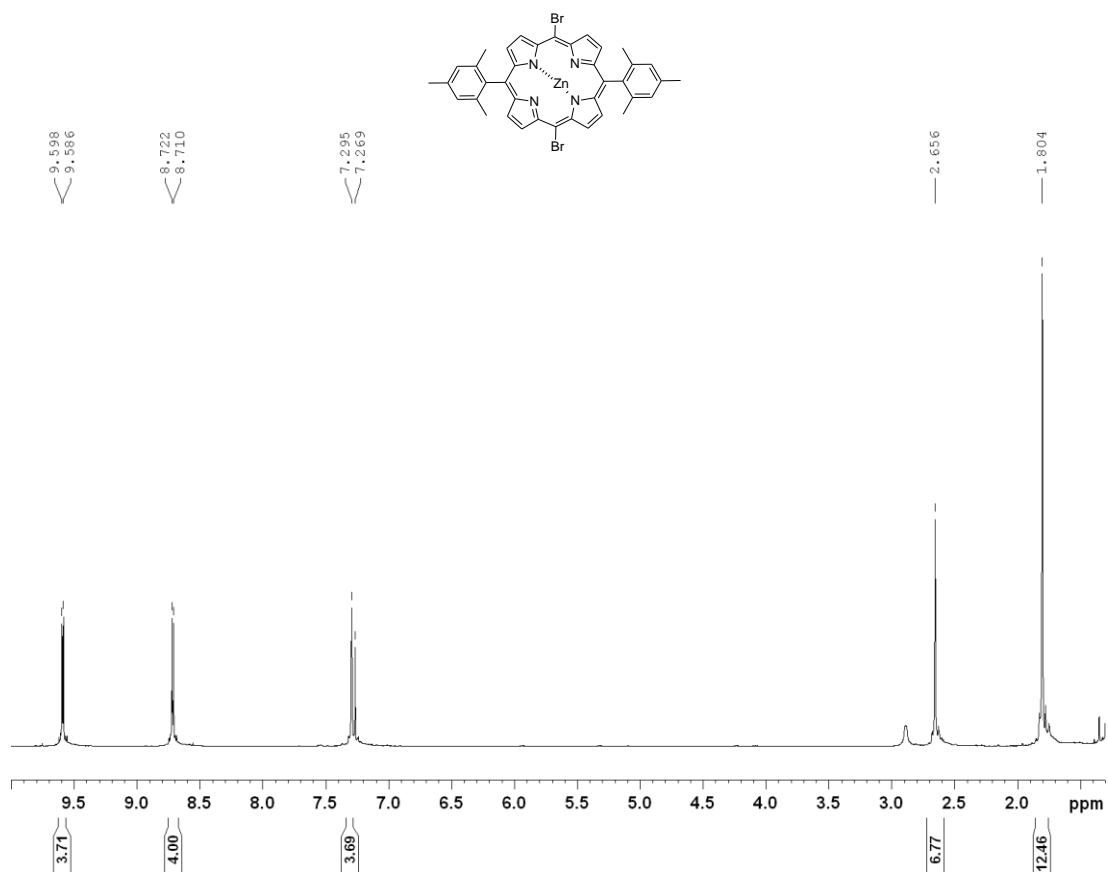


Figure S9. ^1H NMR spectrum (400 MHz, CDCl_3) of [5,15-Dibromo-10,20-dimesitylporphyrinato] zinc (II).

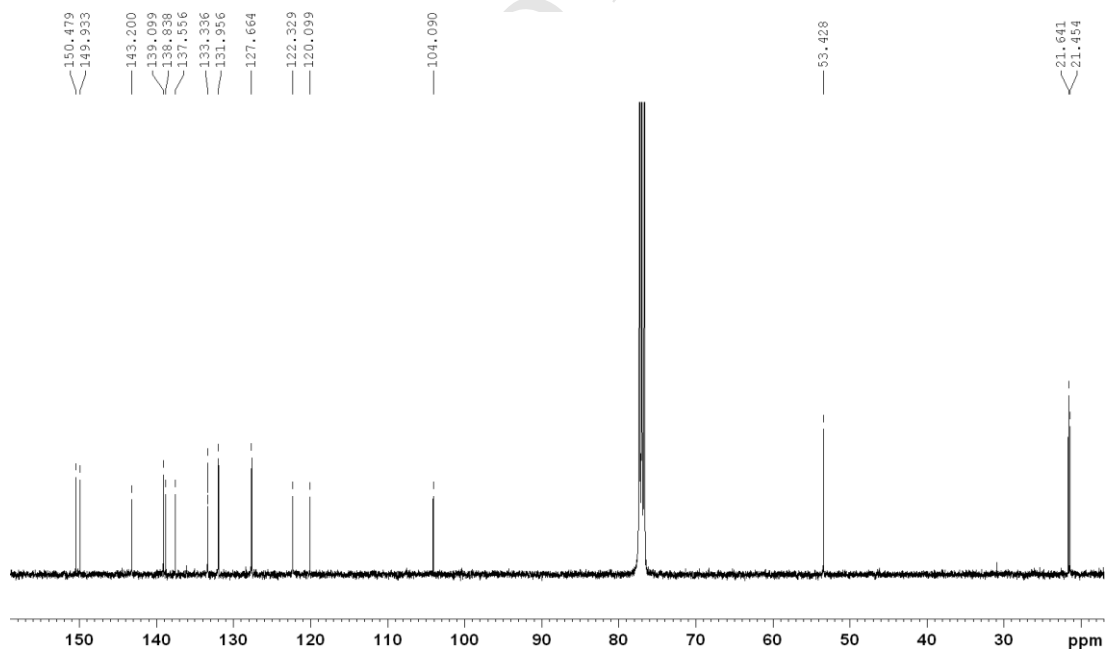


Figure S10. ^{13}C NMR spectrum (100 MHz, CDCl_3) of [5,15-Dibromo-10,20-dimesitylporphyrinato] zinc (II).

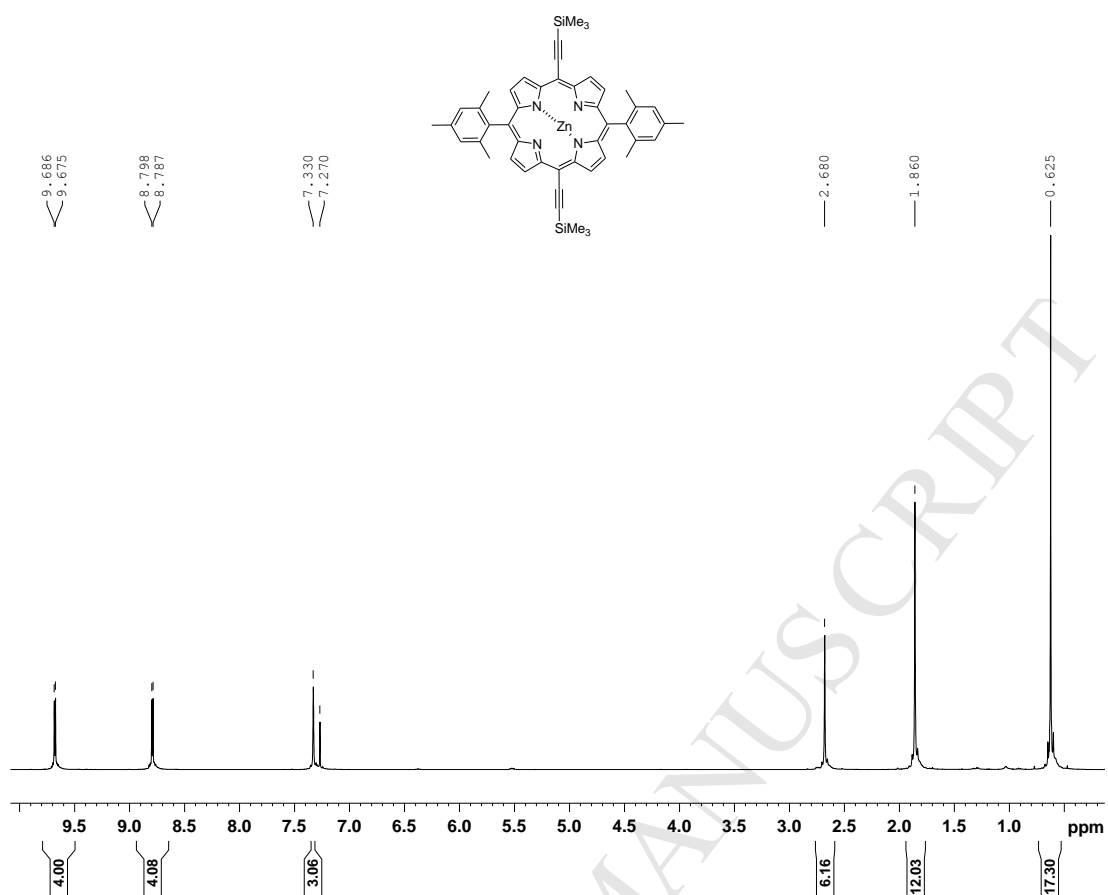


Figure S11. ^1H NMR spectrum (400 MHz, CDCl_3) of **2**.

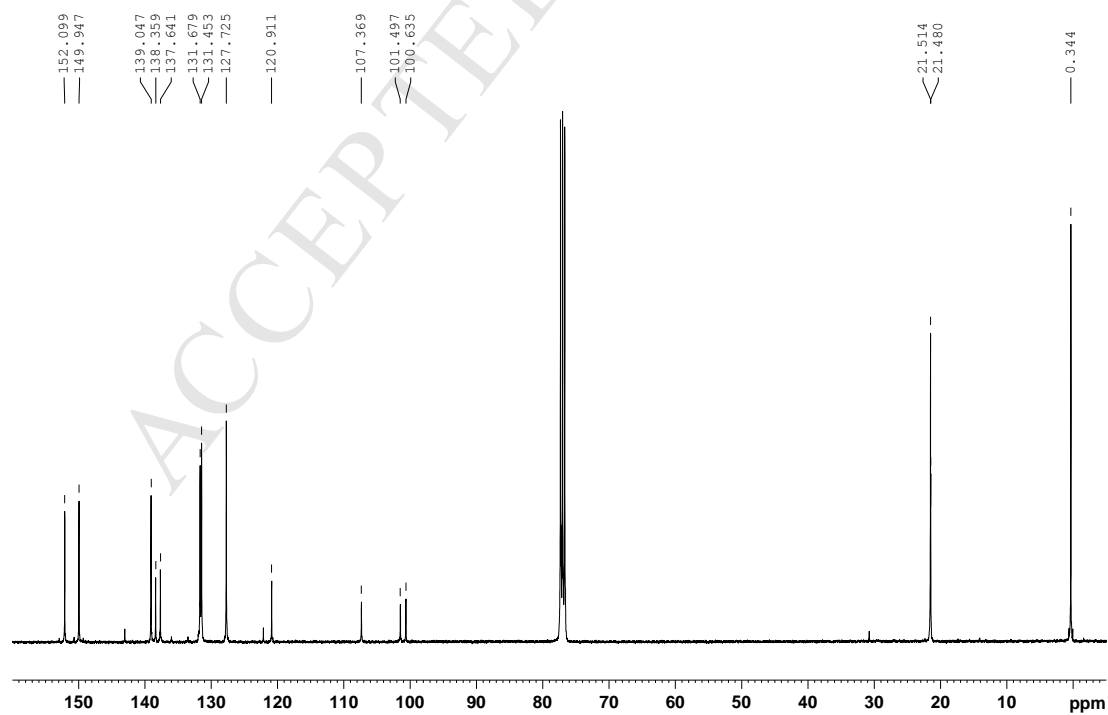


Figure S12. ^{13}C NMR spectrum (100 MHz, CDCl_3) of **2**.

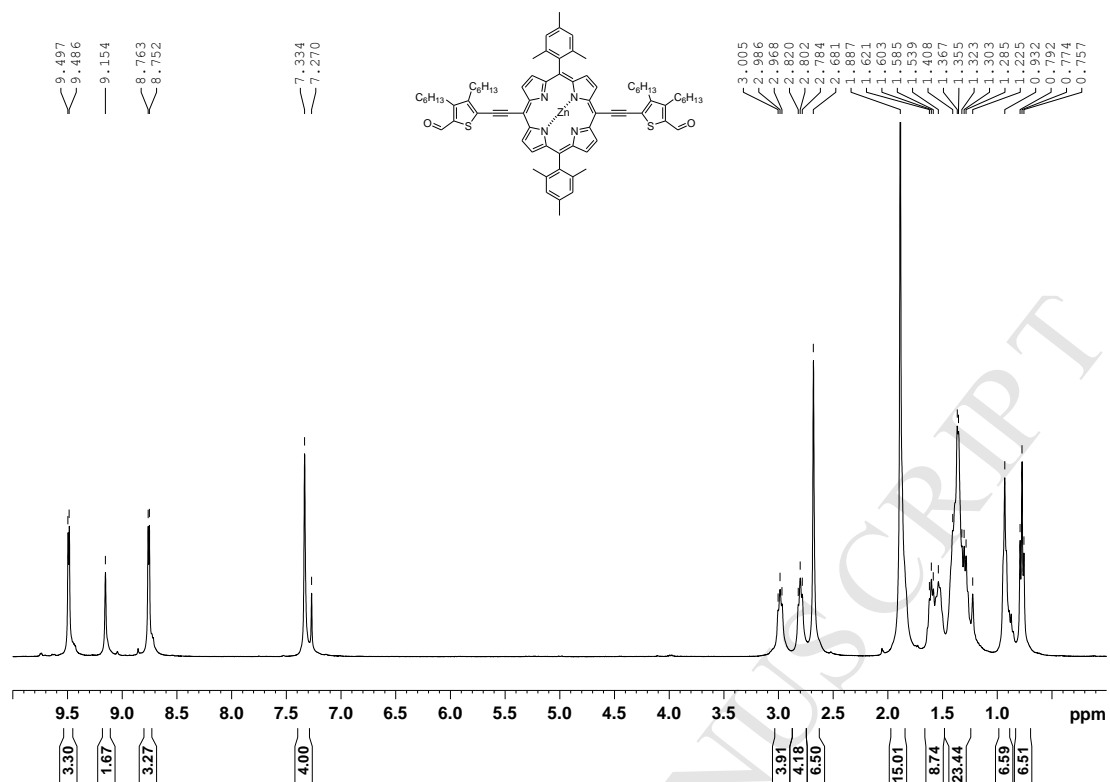


Figure S13. ¹H NMR spectrum (400 MHz, CDCl₃) of **4a**.

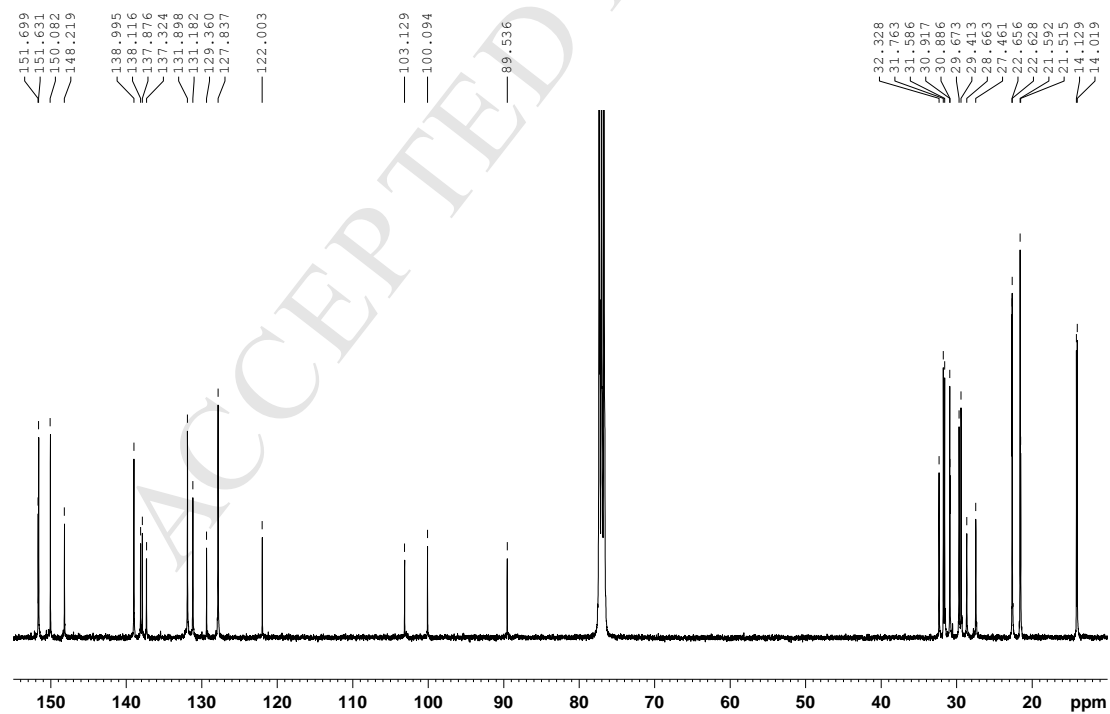


Figure S14. ¹³C NMR spectrum (100 MHz, CDCl₃) of **4a**.

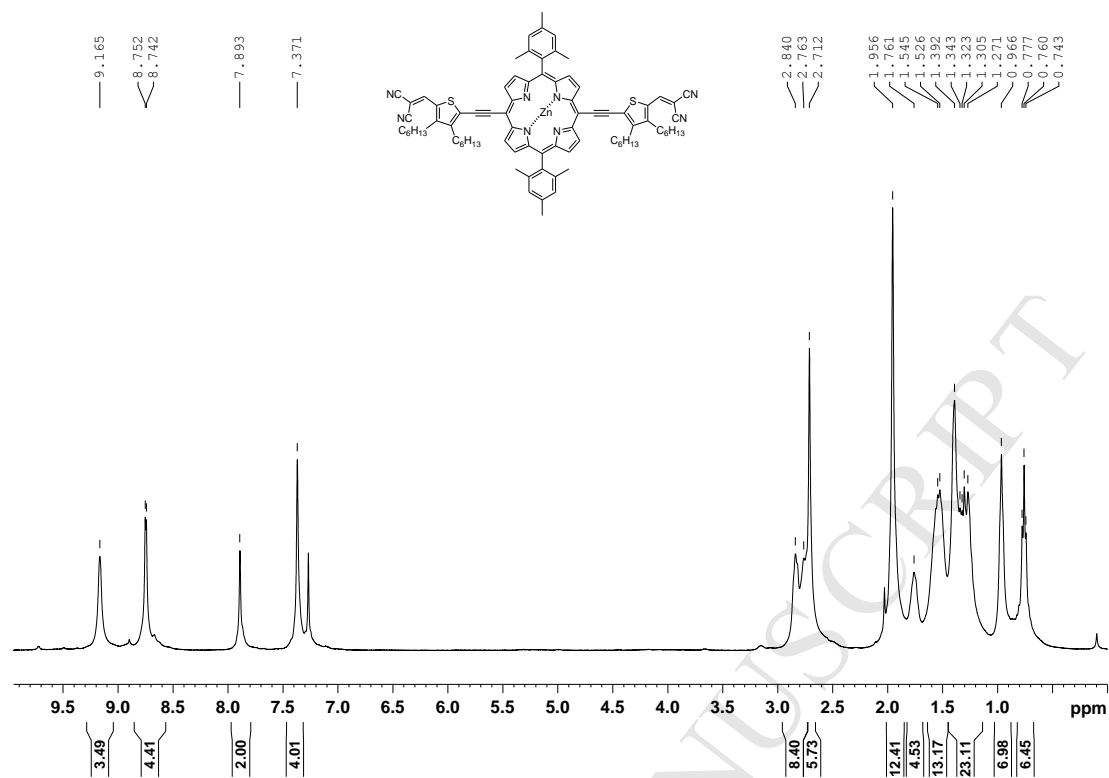


Figure S15. ¹H NMR spectrum (400 MHz, CDCl₃) of **1a**.

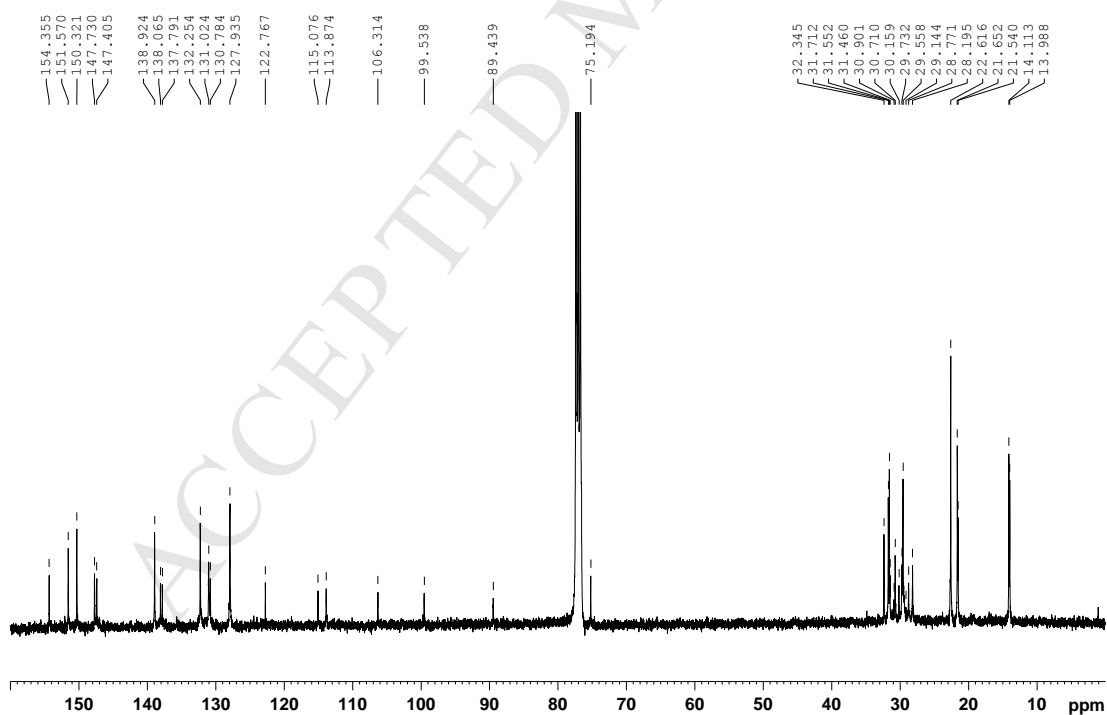


Figure S16. ¹³C NMR spectrum (100 MHz, CDCl₃) of **1a**.

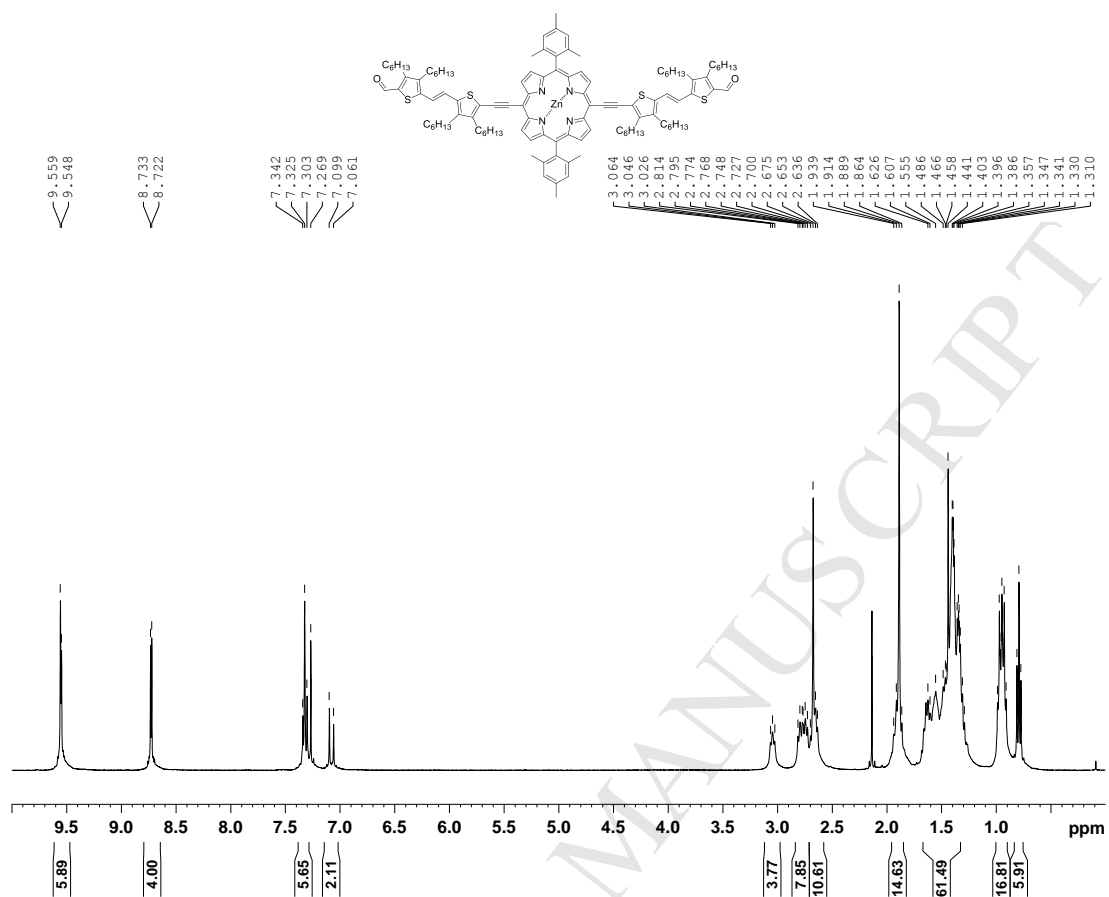


Figure S17. ^1H NMR spectrum (400 MHz, CDCl_3) of **4b**.

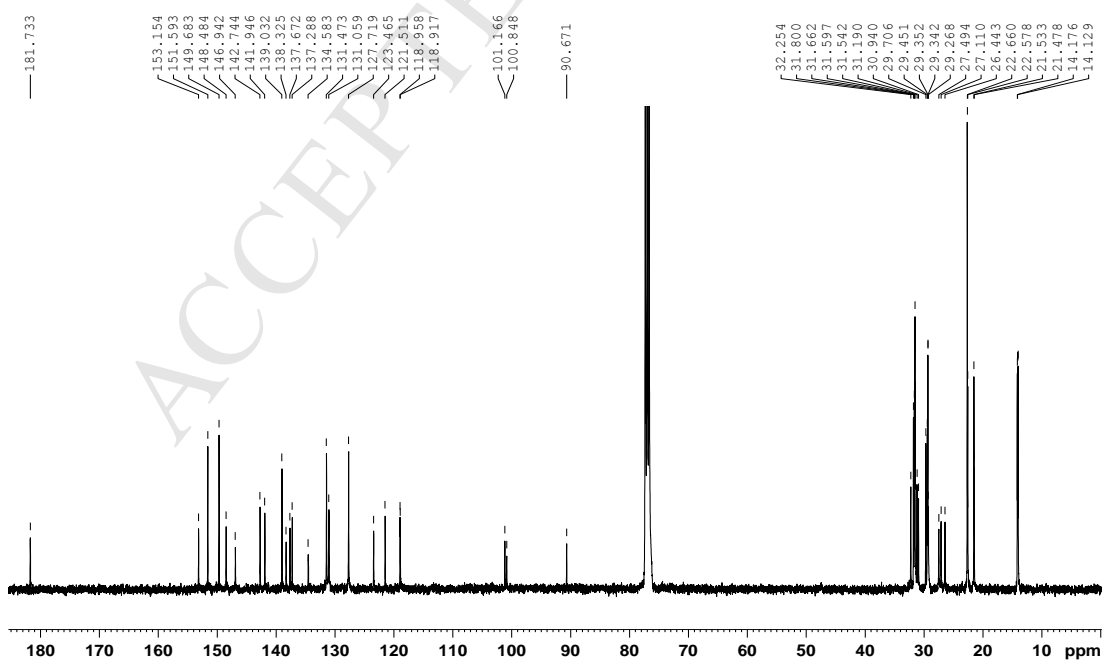


Figure S18. ^{13}C NMR spectrum (100 MHz, CDCl_3) of **4b**.

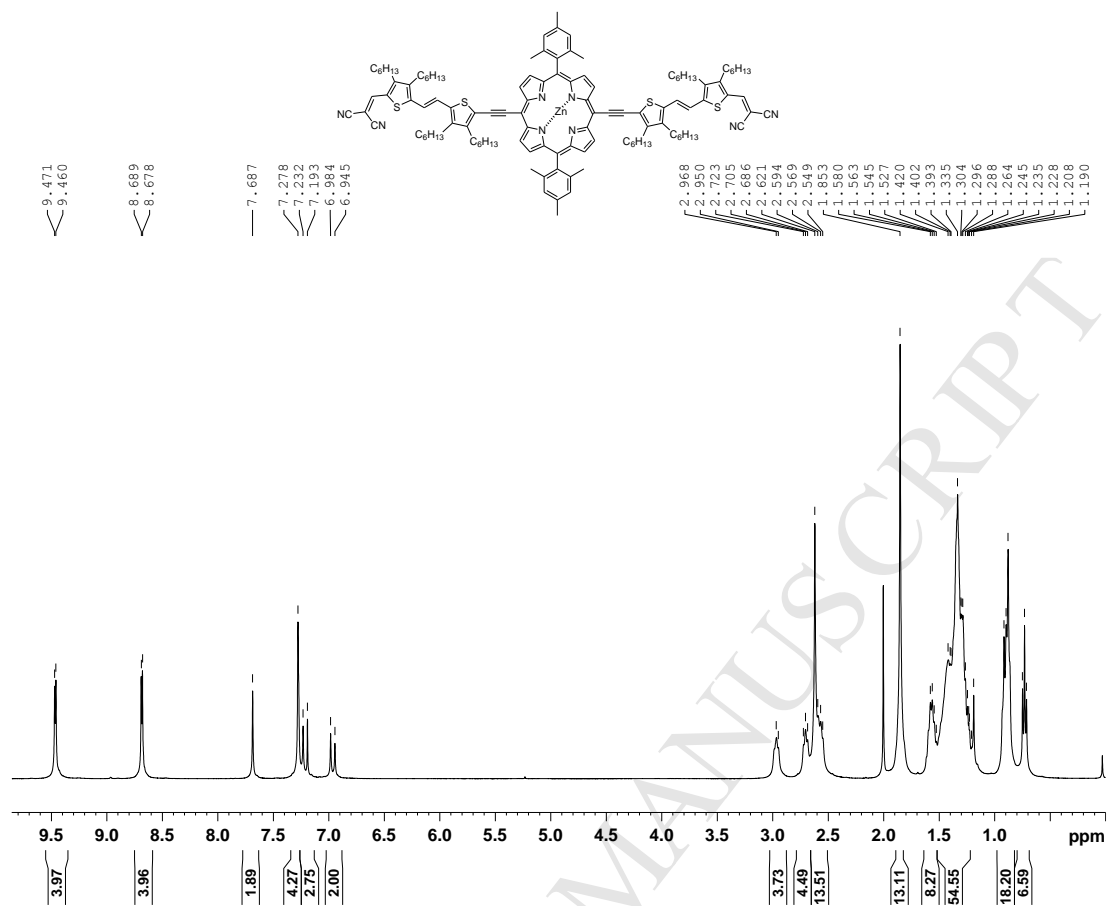


Figure S19. ¹H NMR spectrum (400 MHz, CDCl₃) of **1b**.

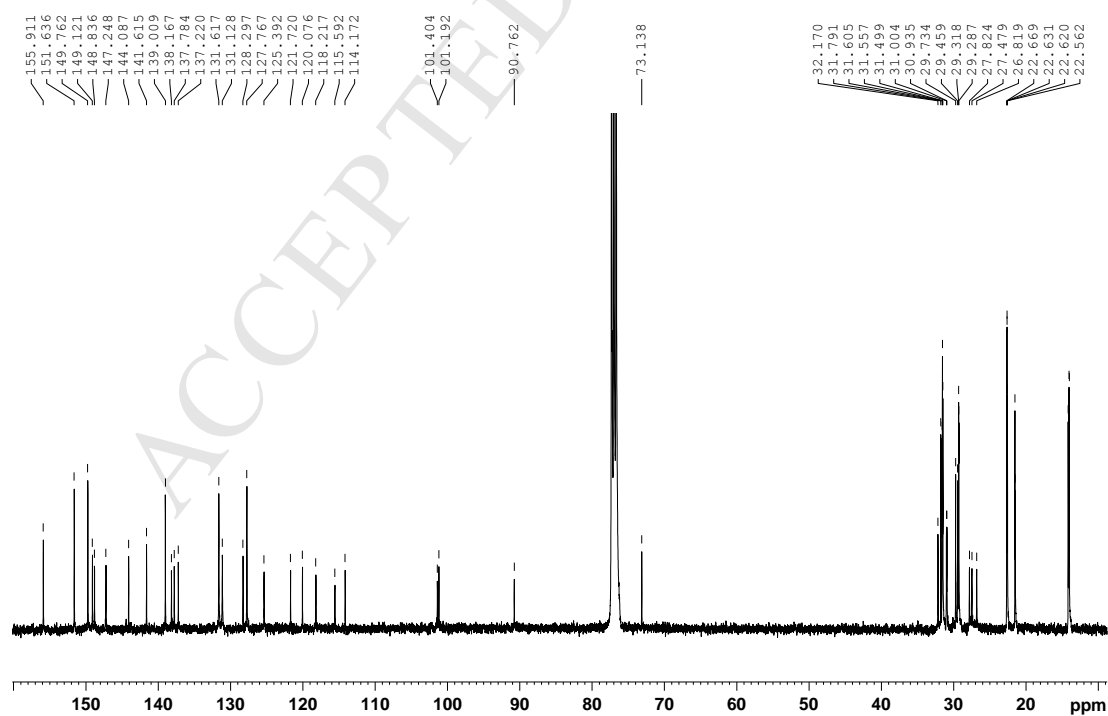


Figure S20. ¹³C NMR spectrum (100 MHz, CDCl₃) of **1b**.

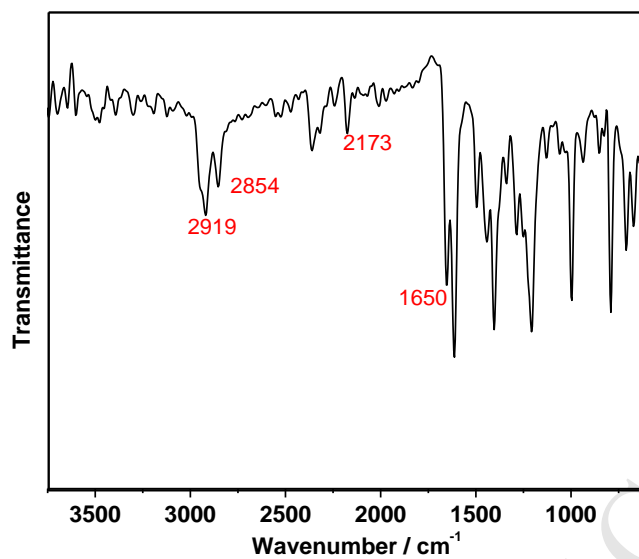


Figure S21. FT-IR spectrum of compound **4a**.

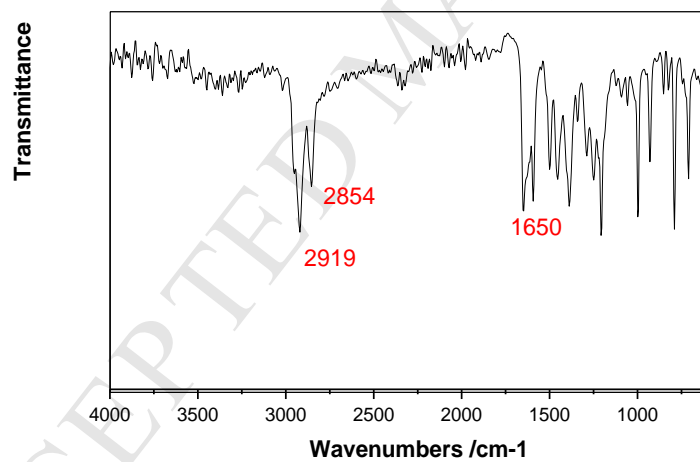


Figure S22. FT-IR spectrum of compound **4b**.

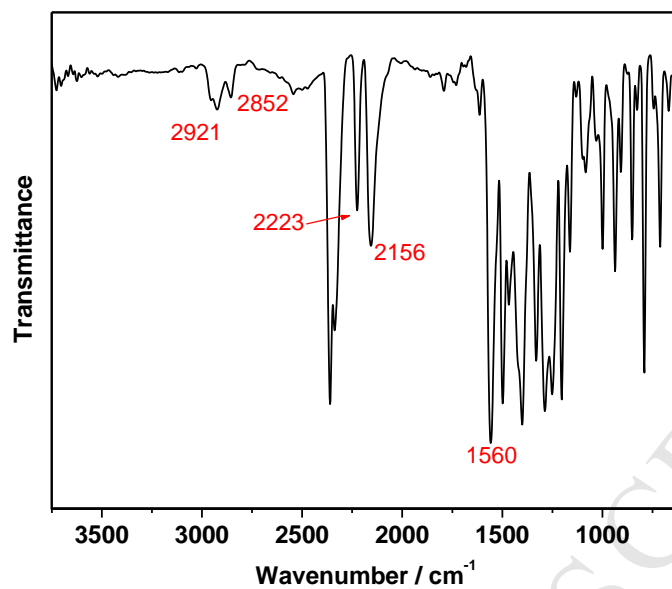


Figure S23. FT-IR spectrum of compound 1a.

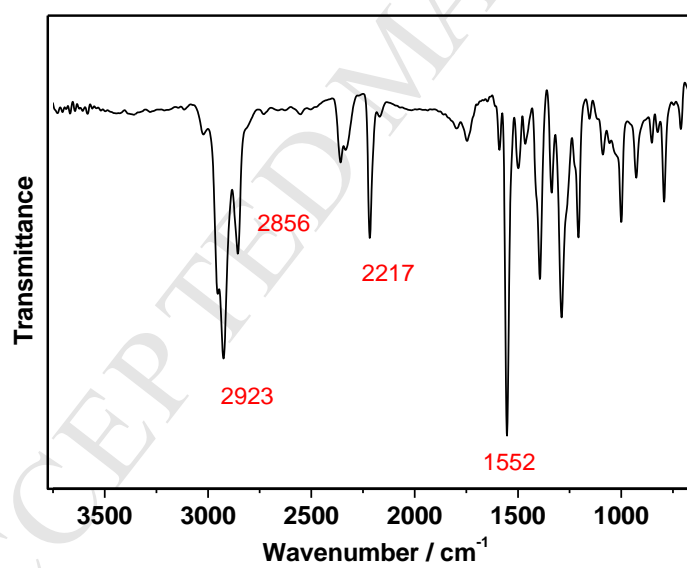


Figure S24. FT-IR spectrum of compound 1b.

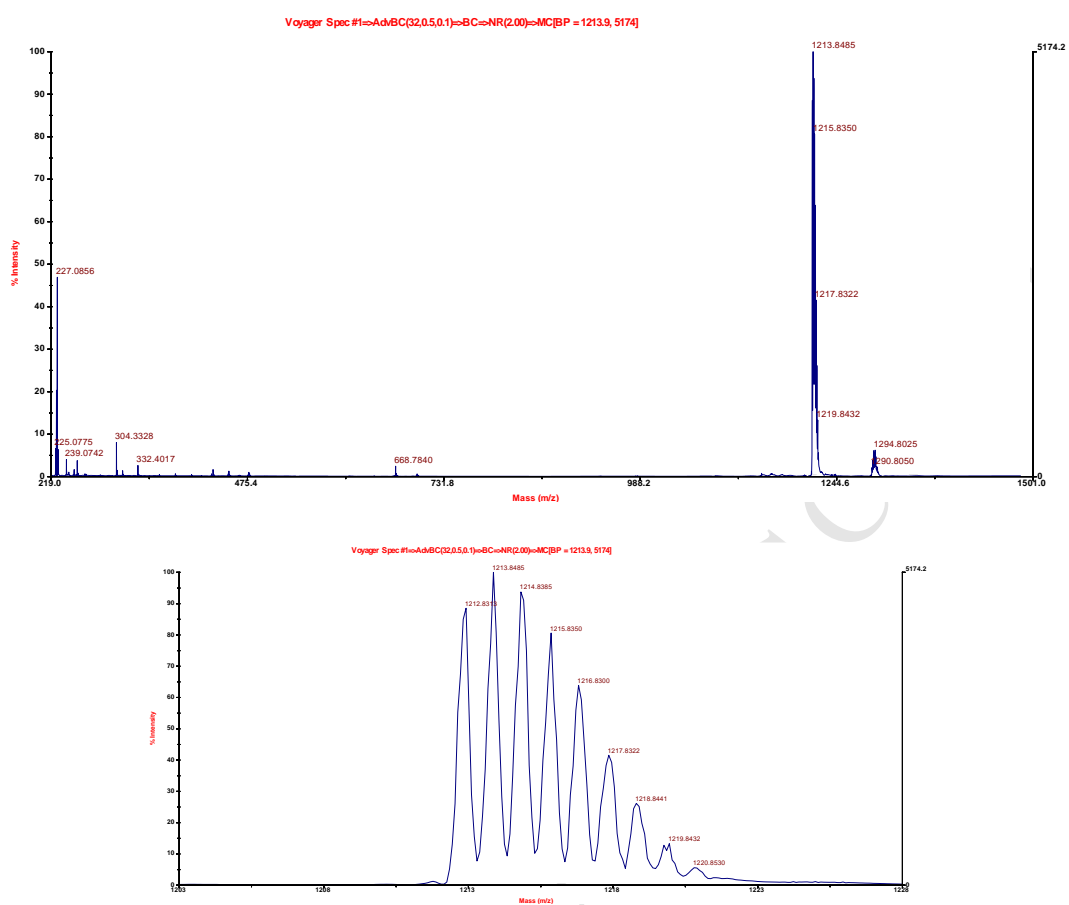


Figure S25. MALDI-MS spectrum of compound **4a** (Matrix: Dithranol).

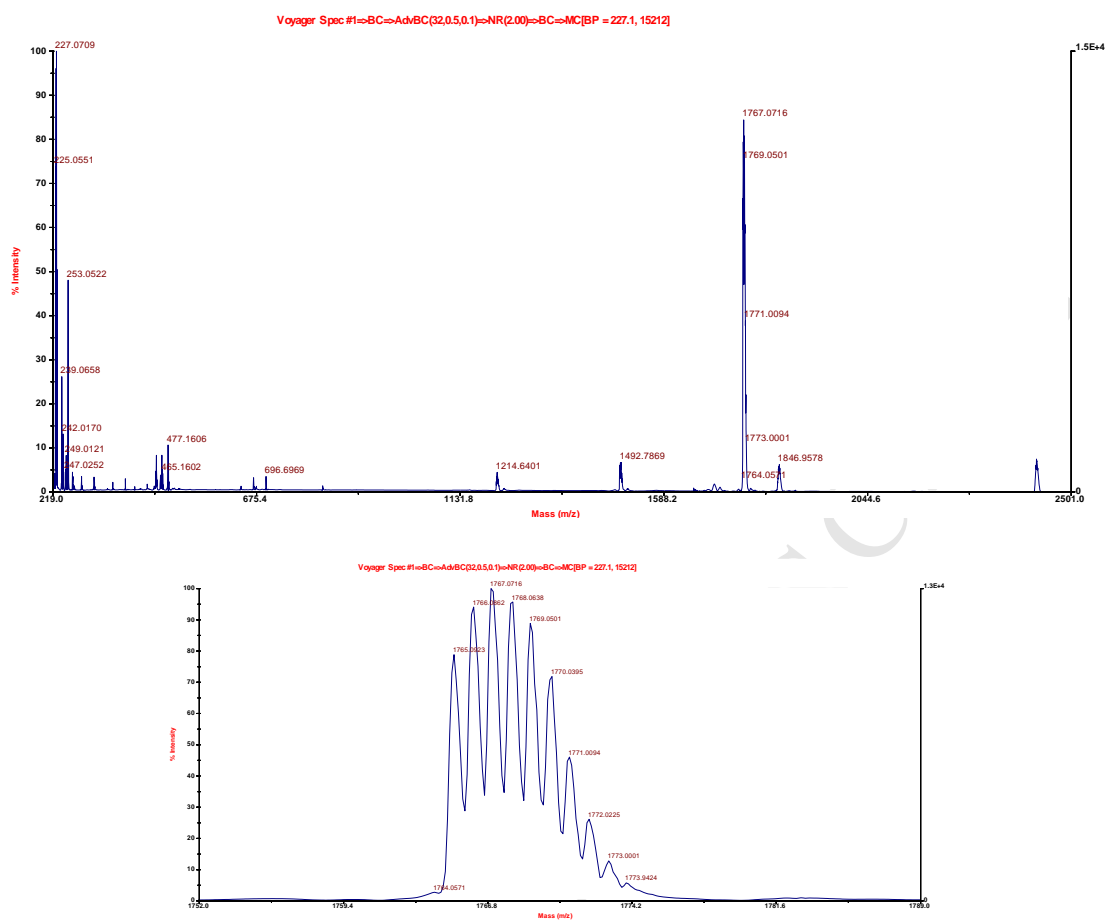


Figure S26. MALDI-MS spectrum of compound **4b** (Matrix: Dithranol).

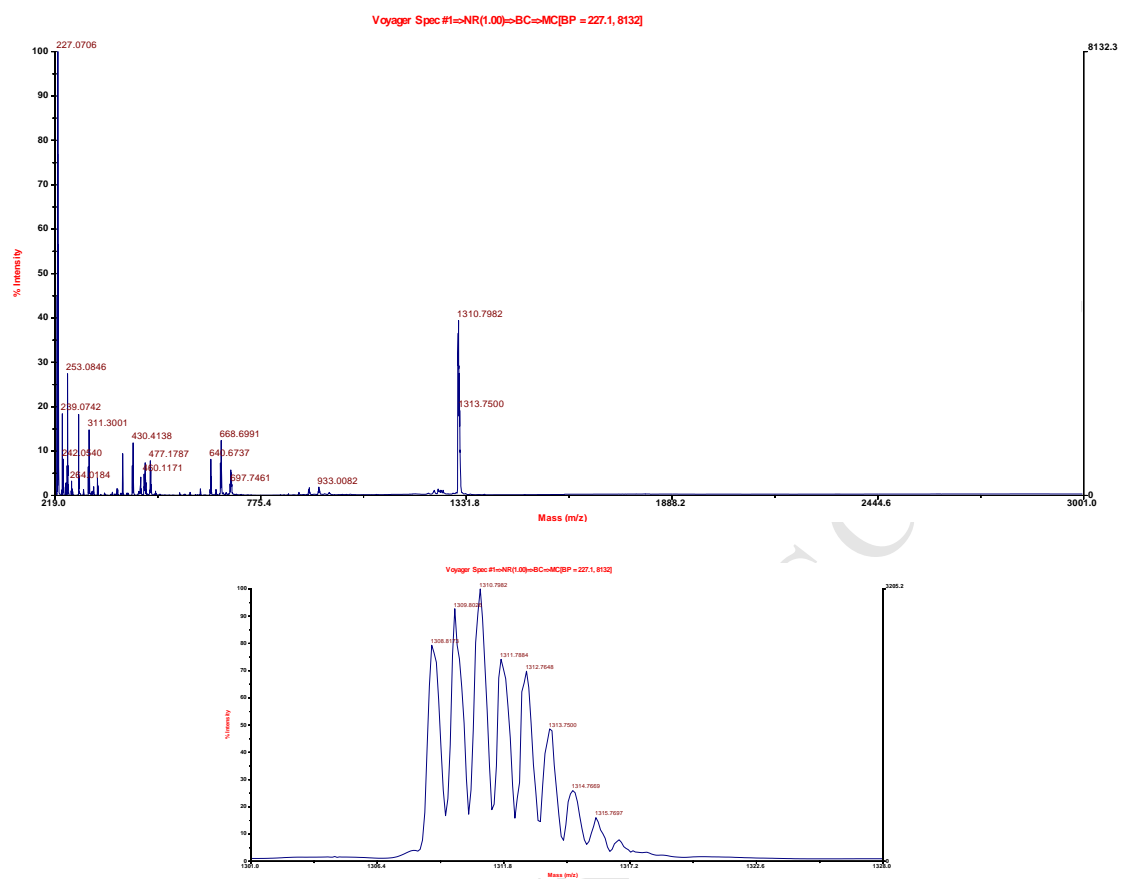


Figure S27. MALDI-MS spectrum of compound **1a** (Matrix: Dithranol).

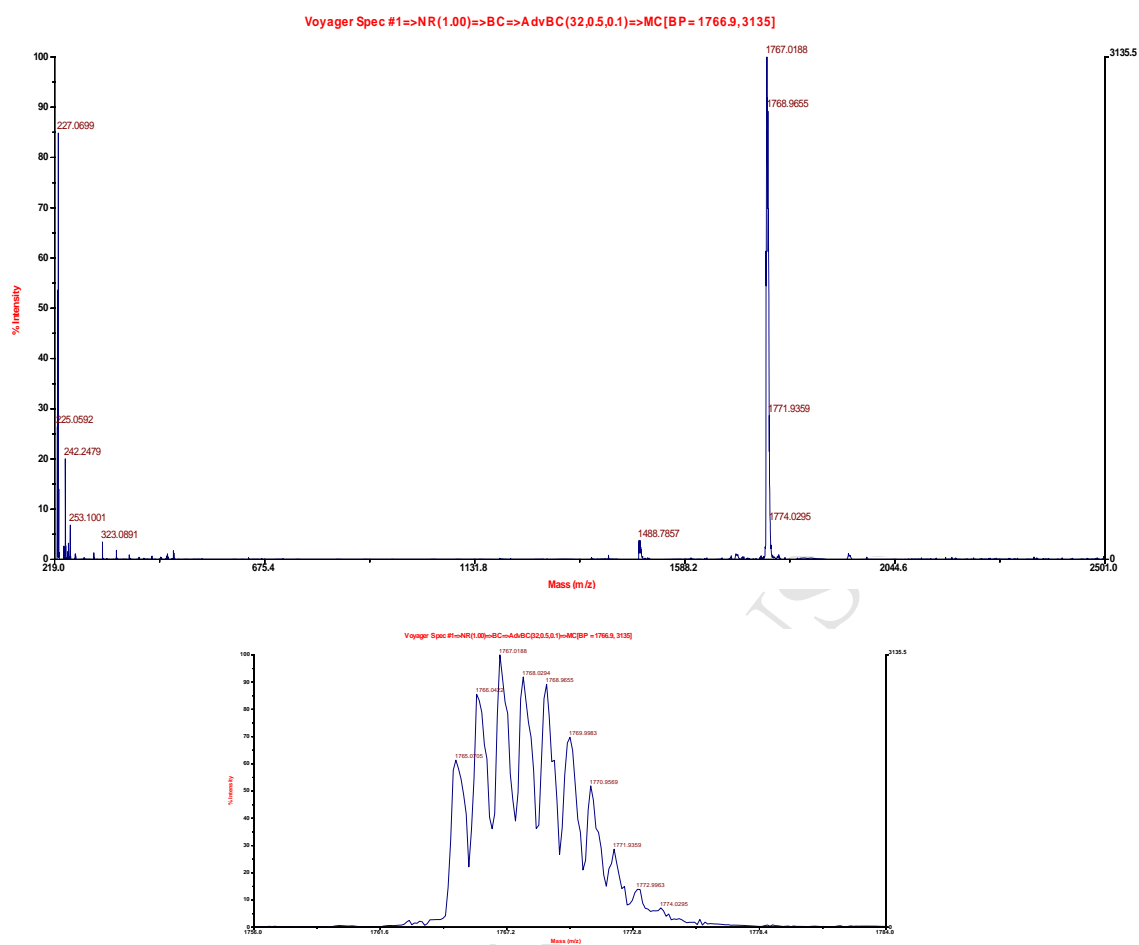


Figure S28. MALDI-MS spectrum of compound **1b** (Matrix: Dithranol).

3. Thermogravimetric analysis

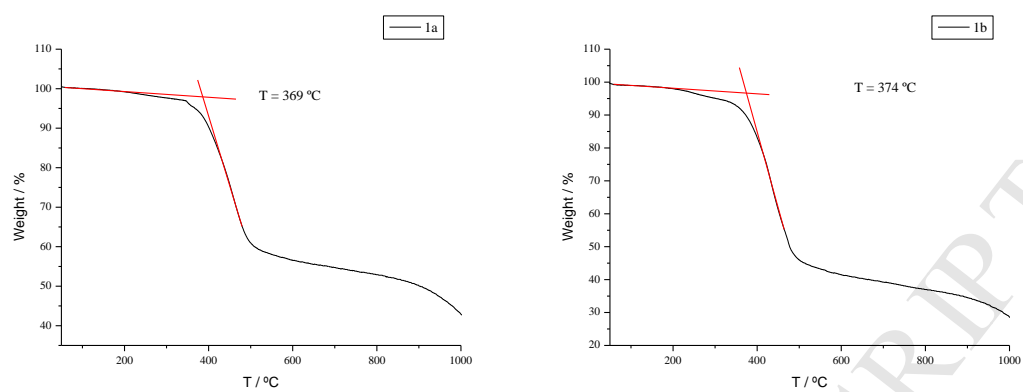


Figure S29. Thermogravimetric analysis of **1a** and **1b**.

4. UV-Visible and emission spectroscopies

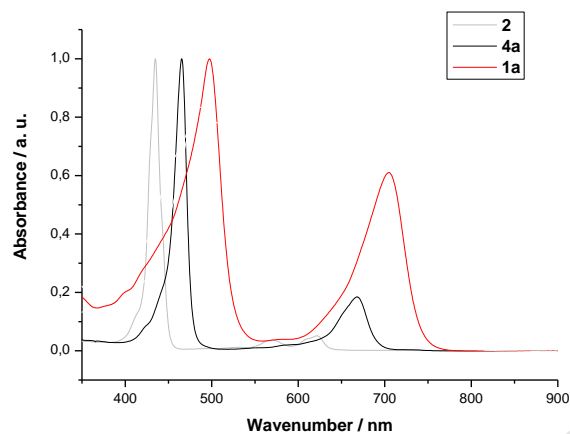


Figure S30. Normalized UV-Vis absorption spectra of compounds **1a** and precursors **2**, **4a** in dichloromethane.

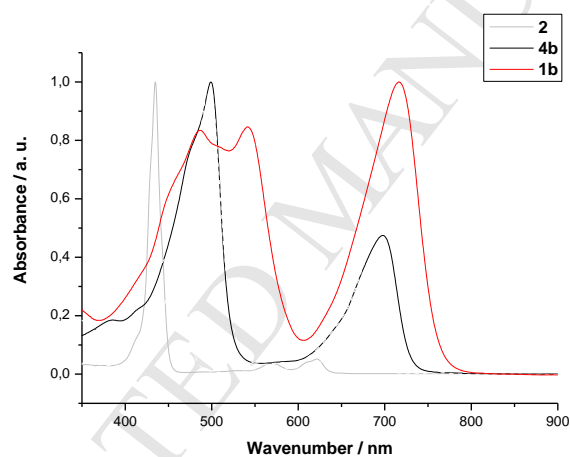


Figure S31. Normalized UV-Vis absorption spectra of compounds **1b** and precursors **2** and **4b** in dichloromethane.

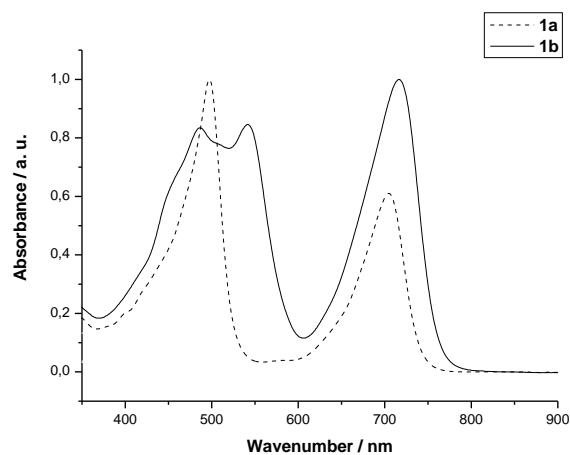


Figure S32. Normalized absorption spectra of **1a** (--) and **1b** (–) in dichloromethane solution (10^{-5} M).

5.

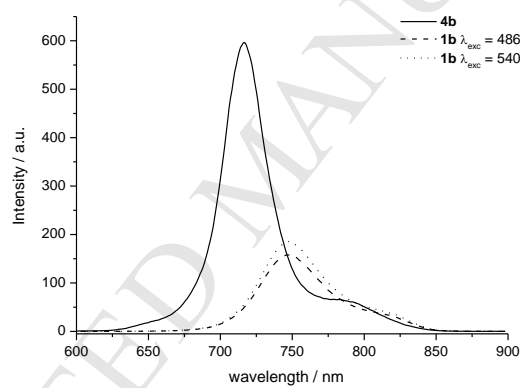


Figure S33. Emission spectra of compound **1b** and **4b** in dichloromethane (10^{-5} M).

6. Square Wave plots

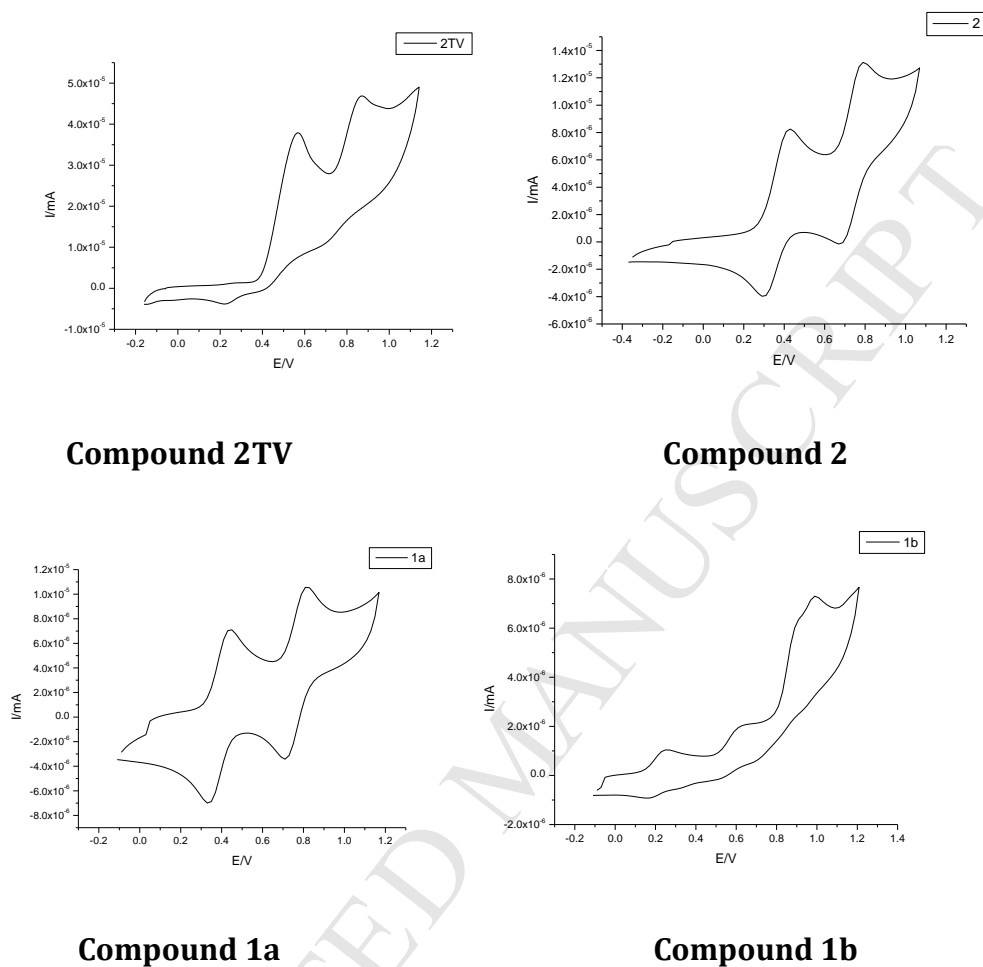


Figure S34. Cyclic Voltammetry of compound **1a-b** and **2TV** and **2** (referred to Fc/Fc^+).

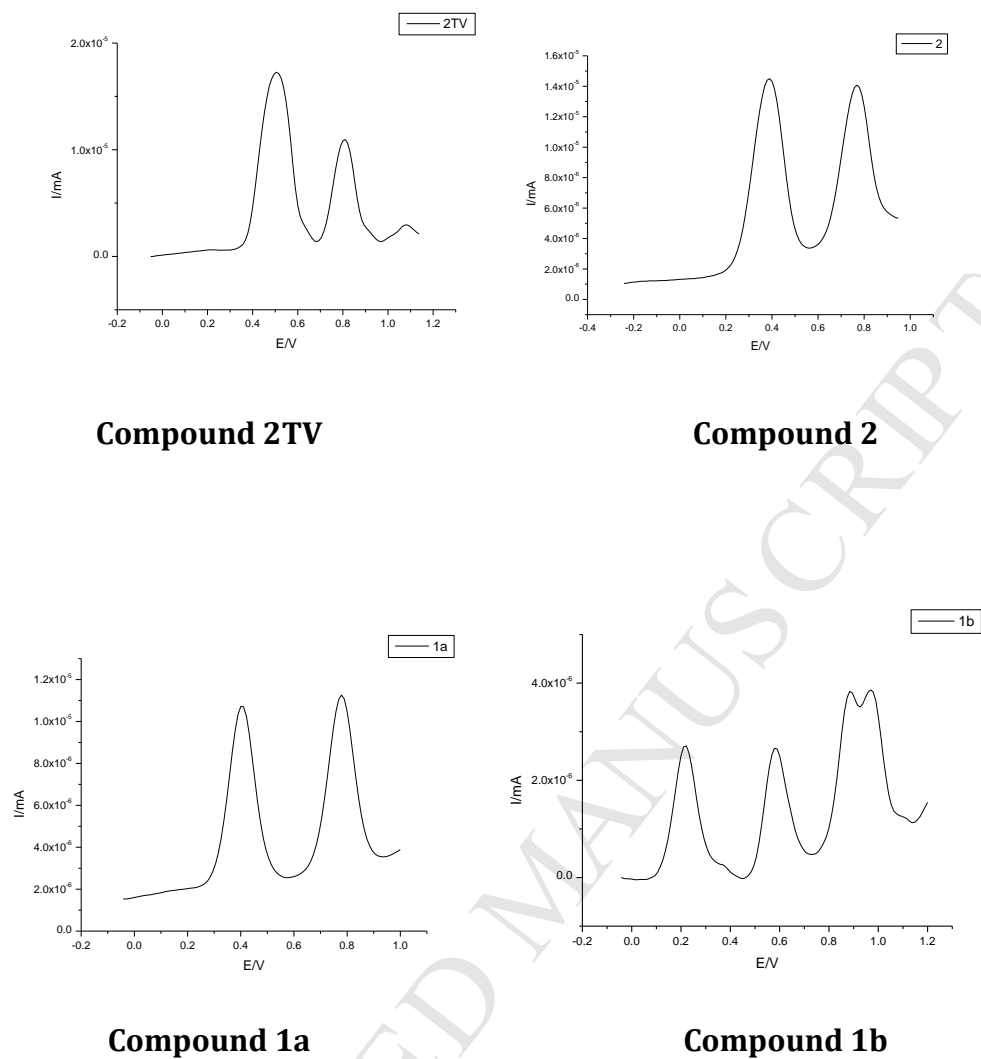


Figure S35. Cyclic Voltammetry of compound **1a** and **1b** and the precursors **2TV** and **2** (referred to Fc/Fc⁺).

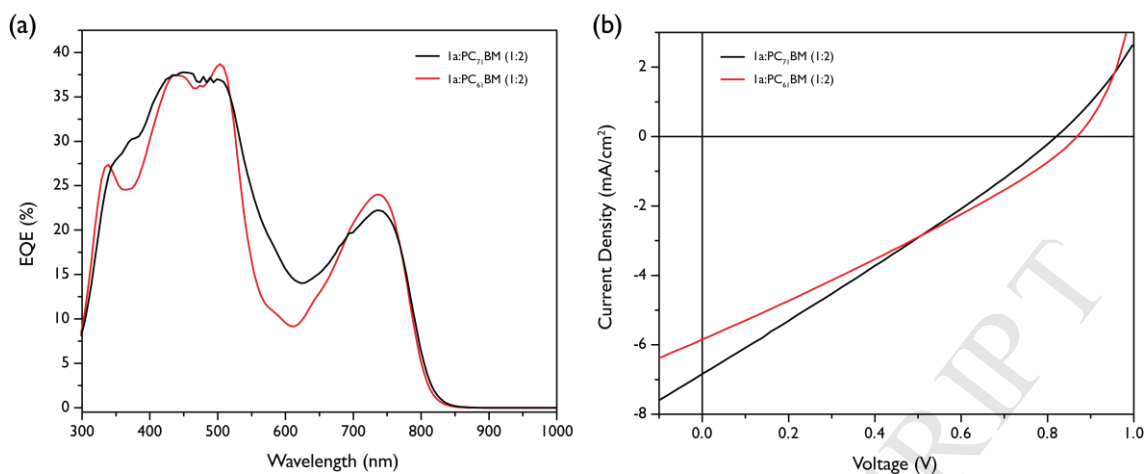
7. EQE and J - V characteristics for 1a:PC₇₁BM (1:2)

Figure S36. EQE (a) and J - V (b) characteristics of the SMBHJ for **1a** blending with PC₆₁BM and PC₇₁BM in a 1:2 ratio.